
THE ECOLOGICAL FORECAST HORIZON REVISITED: POTENTIAL, ACTUAL AND RELATIVE SYSTEM PREDICTABILITY

Marieke Wesselkamp¹ Jakob Albrecht² Ewan Pinnington³ William J. Castillo¹
Florian Pappenberger³ Carsten F. Dormann¹

December 3, 2024

ABSTRACT

Ecological forecasts are model-based statements about currently unknown ecosystem states in time or space. For a model forecast to be useful to inform decision-makers, model validation and verification determine adequateness. The measure of forecast goodness that can be translated into a limit up to which a forecast is acceptable is known as the ‘forecast horizon’. While verification of meteorological models follows strict criteria with established metrics and forecast horizons, assessments of ecological forecasting models still remain experiment-specific and forecast horizons are rarely reported. As such, users of ecological forecasts remain uninformed of how far into the future statements can be trusted. In this work, we synthesise existing approaches, define empirical forecast horizons in a unified framework for assessing ecological predictability and offer recipes on their computation. We distinguish upper and lower boundary estimates of predictability limits, reflecting the model’s potential and actual forecast horizon, and show how a benchmark model can help determine its relative forecast horizon. The approaches are demonstrated with four case studies from population, ecosystem, and earth system research.

1 Introduction

Interest in and use of forecasting models for understanding and managing ecosystems has steadily increased in recent years [1, 2]. The relevance of forecasting earth and environmental systems is driven in parts by two large scale changes: On one hand the warming of the global climate that affects ecosystems of all types. On the other hand the shift in modeling paradigm across various disciplines towards techniques generally summarised under ‘artificial intelligence’, which in earth system modeling most notably happened in the field of weather forecasting [3, 4, 5] and hydrology [6, 7], but also in ecosystem ecology [8, 9]. Forecasts that fall into the realm of ecosystem ecology range from population dynamics [10, 11], to predicting forest productivity on site [12] and landscape scales [13], and also encompass near-term lake [14] or streamflow [6] temperature forecasting. For facilitating communication among scientists but also to decision makers, efforts are made to harmonize ecological forecasting frameworks [15] from assimilation of observations [16, 17], over representation of uncertainties [18] and data archiving [19], to forecast verification [20, 21].

Ecological forecasts have been defined as “the process of predicting the state of ecosystems [...] with fully specified uncertainties, [...] contingent on explicit scenarios” of environmental conditions [22, p.657]. We differentiate further and for the purpose of this study define forecasts as (1) temporal predictions [23] that (2) either operate to inform the wider public [14, 24], or serve as alone-standing tools for targeted applications that inform stakeholders [25] and scientists [26], and that are (3) contingent on verified forecasts of environmental conditions and thus are distinguishing forecasts from projections, contingent on scenarios. The application of a so-defined forecast model outside the scientific discourse and its implications for ecological management leads to a need of quantifying the model forecast horizon and

¹Department of Biometry, University of Freiburg, Germany

²Department of Forest Economics, University of Freiburg, Germany

³European Center for Medium-Range Weather Forecasts, United Kingdom

the system predictability [22, 20]. Understanding the temporal limits of ecological forecasts can inform conservation strategies, such as identifying the time frames within which species population models remain reliable for predicting biodiversity outcomes under different climate scenarios [25]. This is particularly important in adaptive management frameworks, where the timing and duration of interventions can depend on the predictability of ecosystem responses. By establishing a formalized approach to forecast horizons, we aim to provide a standardized tool that can help ecological forecasters and decision-makers assess the temporal reliability of their models.

The concept of ecological forecast horizons was introduced ten years ago [20, 27]. It is a response to the discovery of chaos in nonperiodic deterministic flows of atmospheric dynamics [28, 29], stating that two trajectories of an unstable system with slightly different initial states have a finite predictability. Now, forecast horizons are established in meteorology [27, 30], in hydrology [31], and since the work of Petchey et al. [20] also in ecology [32, 33]. The forecast horizon refers to the time period over which future projections and predictions are made. More specifically, *the forecast horizon is the point in time at which the predictive error becomes large enough that the model no longer meets qualitative or quantitative standards* [20]. From an empirical perspective, forecast performance evaluates the match between predicted and actual outcomes, typically using quantitative metrics [34]. However, forecast performance alone does not necessarily equate to forecast utility, which considers how forecasts inform decision-making in practical contexts. Forecast utility depends on whether the error remains within an acceptable range for a given application [34]. For example, a weather forecast with a 2°C margin of error might be acceptable for general use but could prove inadequate for agricultural decisions, where precision is critical for crop survival. Therefore, while performance sets the technical limits of accuracy [32, 14, 33], utility is determined by the needs and risk tolerance of stakeholders.

An empirical framework to determining forecast horizons analyses forecast performance with metrics that quantify the magnitude of predictive error [35, 34]. Such a framework involves two key assumptions: First, the availability of reference data for model evaluation over the forecast period, which requires observations or re-analyses. Without reference data, theoretical system predictability can be determined, but not model predictive ability [36]. The second assumption is that there is an agreement on a tolerance toward the predictive error up to which forecast performance is actually acceptable [20, 37, 38]. This may come as an ad-hoc accuracy requirement that sets a quantitative cut-off toward the scoring function, related to utility in applied scenarios [39]. Additionally, it is best practice to compare the forecasting models with a benchmark or null model performance [16, 14], based on which a forecast skill horizon can be determined [27].

Within an empirical framework, different forecast horizons can be computed (see figure 1). When reference data are available, the forecast performance can be determined by evaluation with a scoring function over time. An estimate for its actual forecast horizon is the point in time where tolerance toward predictive error, represented by the score, is exceeded [20]. This is comprehensibly demonstrated by Massoud et al. [16] with a plankton community model, displaying the forecast horizon as a function of quantified error tolerance. *Relative* model skill [40] assesses model performance relative to *benchmark* or *null models* [16, 14]. Here, the reference model sets the *ad-hoc* expectation to forecast model performance and a forecast skill horizon can be computed. This was done for example for the geopotential height in ECMWF's forecast ensemble [27]. Finally, without reference data available, the *potential* forecast horizon can be explored by studying potential system predictability, as has been done for example for the Atlantic Meridional Overturning Circulation [41], meridional heat transport [42], and for net primary productivity in marine ecosystems [43, 44]. Forecast performance is here evaluated within a perfect-model framework that erases all but initial conditions uncertainty [45, 46, 36].

In this work, we revisit the concept of forecast horizons to improve model verification in ecological systems beyond chaotic dynamics. We synthesize existing methods to assess the limits of model predictability and system behavior. Our goal is to formalize the distinctions between three types of forecast horizons: potential, actual, and relative. We demonstrate this framework using four case studies that address three different ecological scales: two versions of an ecological population dynamics model, a forest ecosystem model, and an earth system model. Specifically, we demonstrate:

- The motivation for computing forecast horizons with a single-species population model (stochastic Ricker equation).
- The potential forecast horizon using a two-species population model (extended coupled Ricker equation).
- The actual forecast horizon using iLand, an individual-based forest model [13].
- The actual and relative forecast horizon using aiLand, a machine learning emulator for land-surface modeling [47, 9].

These case studies exemplify the diverse applications of forecast horizons in evaluating models across different systems and complexities.

2 Preliminaries

Our formalisation is mainly based on [48] and [49]. The notation follows a statistical tradition: model statements are indicated as \hat{Y} , interpreted as estimates of the true system states Y .

2.1 Definition of forecast models

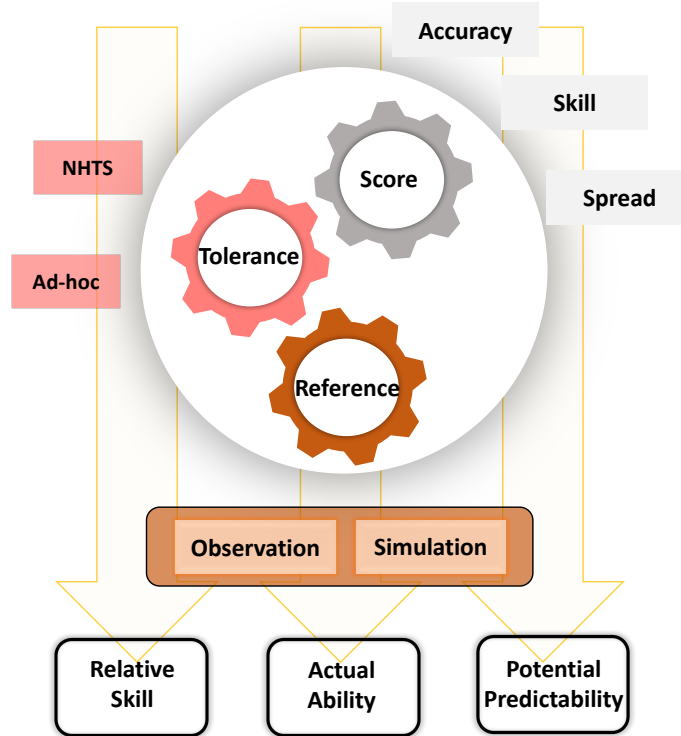


Figure 1: Three main computational hyper-parameters required for empirical forecast horizons are 1) a scoring function that evaluates the match of forecast and reference, 2) a tolerance ϱ toward the scoring function that specifies a cut-off, and 3) an evaluation reference. Based on their composition we classify relative, actual or potential predictability of a system or of a model 2.2.

We define a forecast model, $\mathcal{M}(Y_0, X, \theta)$, as a function or set of functions of initial state variables Y_0 , optional external forcing variables X , and model parameters θ [48]. \mathcal{M} can be a statistical, mathematical, or any other model. The model \mathcal{M} dynamically approximates trajectories of one or more true system states, Y , up to a future point in time τ . In discrete time, \mathcal{M} can be defined iteratively as:

$$\hat{Y}_t = \mathcal{M}(\hat{Y}_{t-1}, X, \theta) + \eta_t \quad \text{for } t = 0, \dots, \tau, \quad (1)$$

where τ is the maximum lead time up to which a forecast is iterated. The lead time τ is pre-defined and can take any integer value. In operational forecasting with numerical models, where $t_0 \ll t$, each forecast is evaluated at $t + \tau$, known as the verification time [50]. In best practice, the choice of τ is guided by the system's predictability limit or the model's predictive ability, as referred by its predictive error ε .

At each time step t , \mathcal{M} returns an estimate \hat{Y}_t of the true system state Y_t . The term η_t represents the dynamical process error, arising from the model's approximation of the true system, and explicitly accounts for the structural uncertainty of the model [49]. Together, components in equation 1 cause what we term the full predictive error ε of the forecast, which is empirically defined using the closest approximation of the "true" process in observation space as the verification

reference Y_t [51]. At any time step t , the predictive error ε_t is given by:

$$\varepsilon_t = \widehat{Y}_t - Y_t. \quad (2)$$

The magnitude of ε_t determines the forecast horizon, as it defines the time limit within which the model can reliably predict the system's behavior [20]. Notably, ε_t grows exponentially in unstable systems [23] and can increase indefinitely in stochastic Markov systems [52].

2.2 Formalisation of the forecast horizon

The forecast horizon, h , is a theoretical concept that suggests a tractable choice of τ , considering ε_t . We formalise h following [20], describing it as an evaluation over lead times using a scoring function and a scoring tolerance within an empirical framework (see overview, figure 1). We define any monotonic function with respect to ε_t as a scoring function $\mathcal{S}(\varepsilon_t)$ [53]. At every time step, t , \mathcal{S} scores the match of \widehat{Y}_t to the reference Y_t . We assume for now that \widehat{Y}_t and Y_t can represent vectors from a forecast and that \mathcal{S} evaluates deterministically. We define the scoring tolerance $\varrho = \varrho(k)$ as a cut-off value toward \mathcal{S} that constitutes the predictive error tolerance. The k can represent any grouping variable, but in this section we assume a simple case without grouping, i.e. k is constant (see Section 3.2 for more details). We formulate a condition that tests at every time step t if score \mathcal{S} exceeds the tolerance ϱ . This can be expressed as a function of time $g(t)$, and with a monotonically declining \mathcal{S} we get

$$g(t) := \mathcal{S}(\varepsilon_t) < \varrho, \quad \text{where } t = 1, \dots, \tau, \quad (3)$$

The first point in time where the condition is true is the estimated forecast horizon \widehat{h} and can be computed as

$$\widehat{h} = \underset{t}{\operatorname{argmin}}(g(t)), \quad \text{where } t = 1, \dots, \tau. \quad (4)$$

When expression 3 is evaluated at every time step t , the result g can be expressed as a step function

$$\gamma = \begin{cases} 0 & \text{if } g(t) \text{ is true} \\ 1 & \text{otherwise} \end{cases} \quad \text{where } t = 1, \dots, \tau. \quad (5)$$

Equation 5 provides the estimate for \widehat{h} at the step where γ changes from 1 to 0. If we assume that we're working in a scenario with observations or re-analysis available for evaluation, i.e. where a reference for Y is available, we get an estimate of the true ε_t with regard to \mathcal{M} and equation 4 estimates the **actual forecast horizon** \widehat{h}_a . Being confronted with the best available reference outside of the model world, \widehat{h}_a provides the natural lower bound of the model's forecast horizon [54].

2.3 Potential predictability

We introduce the upper bound of a model's forecast horizon as the **potential forecast horizon** \widehat{h}_p , which determines the intrinsic predictability limit of the theoretical system [55, 46]. For the computation of \widehat{h}_p the evaluation is set in a so-called perfect-model framework [35, 46], where the model structural uncertainty (represented in equation 1 by η_t) and uncertainty in parameters θ are assumed to be absent. In contrast to h_a , the predictive error ε_t is now caused only by uncertainty in initial conditions Y_0 and X . Technically this means, running the exact same model with slight perturbations of initial states Y_0 , creating a distribution of $i = 1 \dots m$ forecast trajectories $\widehat{\mathbf{Y}}$, i.e. an ensemble with m members. In other words, in the perfect model framework we replace Y_t by the 'perfect' models expectation, $\widehat{\mathbf{Y}}_t$. The predictive error is quantified by step wise evaluating ensemble members against the ensemble mean $\widehat{\mathbf{Y}}$, which gives

$$g(t) := \mathbb{E}_i[\mathcal{S}(\widehat{Y}_{t,i}, \widehat{\mathbf{Y}}_t)] < \varrho, \quad \text{where } t = 1, \dots, \tau \quad \text{and } i \in \{1, \dots, m\}, \quad (6)$$

correspondingly to formula 3. The potential forecast horizon \widehat{h}_p is estimated again using equation 4.

2.4 Relative skill

One way to define a tolerance towards a scoring function is with a (typically low-skill) null or benchmark model that we call \mathcal{R} for reference model [56, 40]. It can be introduced as another term into equation 3. When \mathcal{R} is the long-term mean ('climatology' in meteorology), $\mathcal{R}(Y_t) = \mathbb{E}(Y_t)$, with \mathcal{R} as the persistence at initial forecast time t , $\mathcal{R}(Y_t) = Y_{t-1}$ [40]. \mathcal{R} can also be a numerical benchmark model $\mathcal{R}(Y_0, X, \theta)$, or its climatology or persistence. Evaluation quantifies the

skill of \mathcal{M} relative to \mathcal{R} , where the predictive error of \mathcal{M} , $\varepsilon^{\mathcal{M}}$, is related to the predictive error of \mathcal{R} , $\varepsilon^{\mathcal{R}}$. \mathcal{M} has no skill over \mathcal{R} as

$$\frac{\mathcal{S}(\varepsilon^{\mathcal{M}})}{\mathcal{S}(\varepsilon^{\mathcal{R}})} > 1, \quad (7)$$

with the left hand side (LHS) of the equation being the skill of \mathcal{M} . Skill is an increasing function [56] and with a monotonically declining \mathcal{S} , LHS is large when $\varepsilon^{\mathcal{R}} < \varepsilon^{\mathcal{M}}$. We align the formulation of 7 with equation 3 and reformulate the LHS to the definition of a skill score [40], such that

$$g(t) := 1 - \frac{\mathcal{S}(\varepsilon^{\mathcal{M}})}{\mathcal{S}(\varepsilon^{\mathcal{R}})} < 0 \quad \text{where } t = 1, \dots, \tau. \quad (8)$$

A value of 1 on the LHS indicates perfect skill if and only if $(\varepsilon^{\mathcal{M}}) = 0$. \mathcal{M} has no skill over \mathcal{R} when the LHS drops below 0 [56]. This provides a natural yet liberal choice for ϱ . As with equation 5, evaluation of above equation 8 can be expressed as a step function, where

$$\gamma = \begin{cases} 0 & \text{if } \varepsilon^{\mathcal{M}} > \varepsilon^{\mathcal{R}} \\ 1 & \text{if } \varepsilon^{\mathcal{M}} < \varepsilon^{\mathcal{R}}. \end{cases} \quad (9)$$

Now equation 4 can be applied to get an estimate of the **relative forecast horizon** \hat{h}_r at the step where γ changes from 1 to 0. This approach is the *forecast skill horizon* [27]. Generally, \hat{h}_r is only meaningful for comparisons with the same reference Y_t for scoring with \mathcal{S} in the numerator and in the denominator.

3 Methods

3.1 Scoring functions

The introduced framework assesses the predictive error ε by collapsing all information into a single deterministic measure. This assessment is based on sample estimates [57] and uses a scoring function \mathcal{S} [34]. We propose three scoring functions within this framework, allowing standardised reporting across various forecast horizons.

Mean absolute error The stepwise absolute error $\text{AE}_t = |\varepsilon_t|$ measures accuracy in the unit of the target variable without compensating positive and negative errors, and it is robust to outliers [56]. When shifted by the tolerance ϱ , the scoring function is

$$\mathcal{S}_{\text{AE}_t} = \varrho - |\varepsilon_t|, \quad \text{where } t = 1, \dots, \tau, \quad (10)$$

it behaves similar to a scoring rule [56]: The forecast horizon is reached when $\text{AE}_t < 0$. When ε is a vector and averaged over m ensemble members or samples within a grouping variable, it collapses to the mean absolute error,

$$\mathcal{S}_{\text{MAE}_t} = \mathbb{E}_i[\varepsilon_t] = \frac{1}{m} \sum_{i=1}^m \varepsilon_{t,i}, \quad \text{where } t = 1, \dots, \tau \quad \text{and } i \in \{1, \dots, m\}. \quad (11)$$

For averaging over a forecast ensemble, we call this the mean ensemble error (see section 4.1).

Mean absolute error skill score Skill scores compare the accuracy of the forecast model \mathcal{M} to that of a reference model \mathcal{R} [56, 40]. With the MAE, the scoring function of skill can be defined as

$$\mathcal{S}_{\text{MAE-SS}_t} = 1 - \frac{\text{MAE}_{t,\mathcal{M}}}{\text{MAE}_{t,\mathcal{R}}}, \quad \text{where } t = 1, \dots, \tau. \quad (12)$$

It indicates perfect skill of \mathcal{M} if $\text{MAE-SS}_t = 1$ and skill of \mathcal{M} no better than \mathcal{R} if $\text{MAE-SS}_t < 0$.

Potential prognostic predictability The upper limit of model predictability can be determined with Potential Prognostic Predictability (PPP) [44]. With PPP, the natural variance of the model is compared to the variance of its forecast distribution. This distribution is usually generated as an ensemble forecast in a perfect-model framework with the assumptions that parameters and model structure are optimal. Ensemble members are simulated with a slight perturbation of initial system states. PPP is defined for spatial analyses with one ensemble forecast per grid cell that are subsequently averaged over grid cells. For our demonstration we simplify its formulation to a single point or cell. With

the ensemble mean from equation 6, the scoring function with PPP can be expressed as

$$S_{\text{PPP}_t} = 1 - \frac{1}{(n-1)} \sum_{i=1}^n \frac{(\hat{Y}_{t,i} - \bar{\hat{Y}}_t)^2}{\sigma_c^2}, \quad \text{where } t = 1, \dots, \tau. \quad (13)$$

The expression subtracted from 1 are the stepwise ensemble variances of the n ensemble members, normalised by the total long-term variance σ_c^2 [27] [44]. PPP indicates perfect predictability at 1 and no predictability if $\text{PPP}_t < 0$.

3.2 Scoring tolerance

Outside of equation 8, the tolerance ϱ towards the score that quantifies the predictive error remained undefined. Even when using equation 8, this does not exclude the definition a more rigorous ϱ as tolerance to skill. We distinguish two non-exclusive approaches that are A) a user perspective that requires quantitative expectations to define a tolerated forecast value ad-hoc [34, 20], and B) a technical perspective that defines tolerance by the statistical significance of forecast quality.

Ad-hoc expectation Depending on the forecast context, ϱ may be available as an ad-hoc expectation of model accuracy [20]. In these cases, ϱ has the unit of the forecasted state variable, e.g. Kelvin for soil temperature or Metres for dominant stand height. For example, in coupled earth system models, the magnitude of predictive error on soil temperature that leads to instable land-atmosphere interactions is known to be above three Kelvin [39]. Another example are forecasts of forest productivity based on stand yield tables that classify forest productivity directly by the expected economic profit. When ϱ is determined across groups within a grouping variable k (such as species, see section 4.3 for an example), it becomes a function $\varrho(k)$ of that variable. Alternatively, when the forecast is a distribution of ensembles from i.e. initial state perturbation or parameter propagation, the tails of this distribution can define the ad-hoc value. We specify the tolerance as an interval within which observations are expected to fall. A relatable choice is the 95% confidence interval that under normal assumptions can be approximated with twice the ensemble standard deviation, or with respective percentiles otherwise.

Null hypothesis significance testing Equations 13 and 16 compare sample statistics. Significance of their difference can be assessed with null significance hypothesis testing [58, 44]. We conduct this approach with the Potential Prognostic Predictability (PPP). Significant PPP values are determined by testing the null hypothesis that $\mathbb{E}^2(\hat{Y}_t^{\mathcal{M}}) \neq \mathbb{E}^2(\hat{Y}_t^{\mathcal{C}})$, where $\mathbb{E}^2(\hat{Y}_t^{\mathcal{M}})$ and $\mathbb{E}^2(\hat{Y}_t^{\mathcal{C}})$ are step-wise ensemble variance and total climatological variance, respectively. We test for differences in variances with an F-test at a significance level of $\alpha = 0.05$. The F-value that defines the given distribution constitutes the tolerance ϱ toward PPP. The forecast horizon is reached as

$$\text{PPP} > 1 - \frac{1}{F(\text{df}_{\text{ensemble}}, \text{df}_{\text{climatology}})}. \quad (14)$$

The ensemble degrees of freedom for the F-statistics are $\text{df}_{\mathcal{M}} = m - 1$, where m is the ensemble size, and degrees of freedom of the climatology $\text{df}_c = \frac{\tau}{(1-\beta)/(1+\beta)}$, with β being the lag-1 temporal autocorrelation [42]. Monte Carlo permutation techniques offer a non-parametric alternative to testing for significant differences in skill scores [58].

4 Case studies

We motivate and demonstrate the computation of potential, actual, and relative forecast horizon in four case studies from population ecology, ecosystem ecology and earth system research. Our initial case study motivates the concept, while each subsequent showcases one of the three forecast horizons with application specific choices to computational components. The models vary in type, state variable, forecast range and dynamic properties (see Table 4). For detailed model descriptions and methodology we refer to the Appendix. These case studies were selected to demonstrate the versatility of the forecast horizon framework across different ecological contexts. The population ecological models represent small-scale, high-frequency dynamics, making it ideal for exploring the limits of predictability in stochastic and chaotic systems. The forest ecosystem model operates on decadal timescales and integrates complex external drivers such as climate and soil properties, providing an example of forecasting at larger spatial and temporal scales. Finally, the machine learning ensemble-based land surface model offers a cutting-edge application in forecasting, highlighting how the forecast horizon concept can be applied to advanced, data-driven models.

Table 1: Overview of the key characteristics of three different modeling approaches used in the case studies with the stochastic Ricker (S-Ricker) and the coupled Ricker (C-Ricker) model, iLand, and aiLand and of the choices of the computational components to compute their forecast horizons. We classify the horizon from the S-Ricker model as potential based on the simulation reference we use, even though we strictly define it only for the show case with C-Ricker.

		S-Ricker	C-Ricker	iLand	aiLand
Model	<i>Model type</i>	Mathematical	Mathematical	Process-based	ML-Ensemble
	<i>State variable</i>	Population size [-]	Population size [-]	Dominant height [m]	Soil temperature [K]
	<i>Driving dynamic</i>	Internal	Internal / External	External	External
Forecast	<i>Time scale</i>	Generational	Seasonal	Decadal	Medium-range
	<i>- representation</i>	Discrete	Discrete	Discrete	Discrete
	<i>Spatial scale</i>	Local	Local	Regional	Local
	<i>- representation</i>	Single point	Single point	Multiple points	Single point
Evaluation	<i>Reference</i>	Simulations	Simulations	Observations	Observations
	<i>Statistic</i>	Spread	Variance	Mean	Mean
	<i>Scoring function</i>	AE	PPP	MAE	MAE(-SS)
	<i>Tolerance</i>	Ad-hoc	NHST	Ad-hoc	Ad-hoc / Null Model
Horizon		<i>Potential</i>	Potential	Actual	Actual / Relative

4.1 Motivating forecast horizons

Setting The forecast model $\mathcal{M}(Y_0, X, \theta)$ is a single-species Ricker-type equation that simulates a growth dynamic. The Ricker model is a discrete-time dynamical model commonly used in theoretical community ecology to describe population growth as a functional response [59]. The estimated state variable \hat{Y} is the population size relative to an environment’s carrying capacity and evolution of \hat{Y} over time represents generational turnover of the population. With Monte carlo error propagation, we iteratively simulate \hat{Y} from Y_0 until \hat{Y}_τ with stochastic parameters and initial conditions from uni-variate Gaussian distributions with fixed variances of 12%. The reference Y are simulated observations from that same model (for more model details, see Appendix). Over 150 generational lead times, we forecast with an ensemble of 500 trajectories.

Forecast horizon We define the forecast horizon as the moment in time where observations are not anymore included in the 95% confidence interval of the ensemble distribution which hence constitutes our ad-hoc choice for ϱ . Because we evaluate the model forecast against simulations, we classify this horizon as potential, even though it does not strictly fall into our definition of potential predictability. This horizon is related to the relationship between the ensemble spread and the mean ensemble error that is here equivalent with the average predictive error ε (see section 3.1) [57]. Scoring function \mathcal{S} to compute the step-wise mean ensemble error $\bar{\varepsilon}_t$ is the member-wise absolute error of simulated observations and the ensemble spread σ . We compute σ as the step-wise sample estimate of the ensemble standard deviation. Assuming normality, the confidence interval is approximated as 2σ and used as tolerance to $\bar{\varepsilon}_t$ (see figure 2, panel B). The horizon is reached as $\bar{\varepsilon}_t$ exceeds ϱ , i.e. when observations are outside of the 95% confidence interval.

Results The spread of the forecast ensemble increases up to approximately 50 generations after which it converges (see panel B). This is where the relative population sizes reaches carrying capacity and the average population becomes stable (panel A). The step-wise mean ensemble error $\bar{\varepsilon}_t$ increases over a similar time period, after which it shows large deflections that exceed the tolerance ϱ , i.e. the 95% confidence interval of the ensemble mean (panel B). Evaluation of the distance of ϱ and $\bar{\varepsilon}_t$ over time (see equation 10) indicates a forecast horizon after > 60 generations where $\bar{\varepsilon}_t$ exceeds ϱ for the first time.

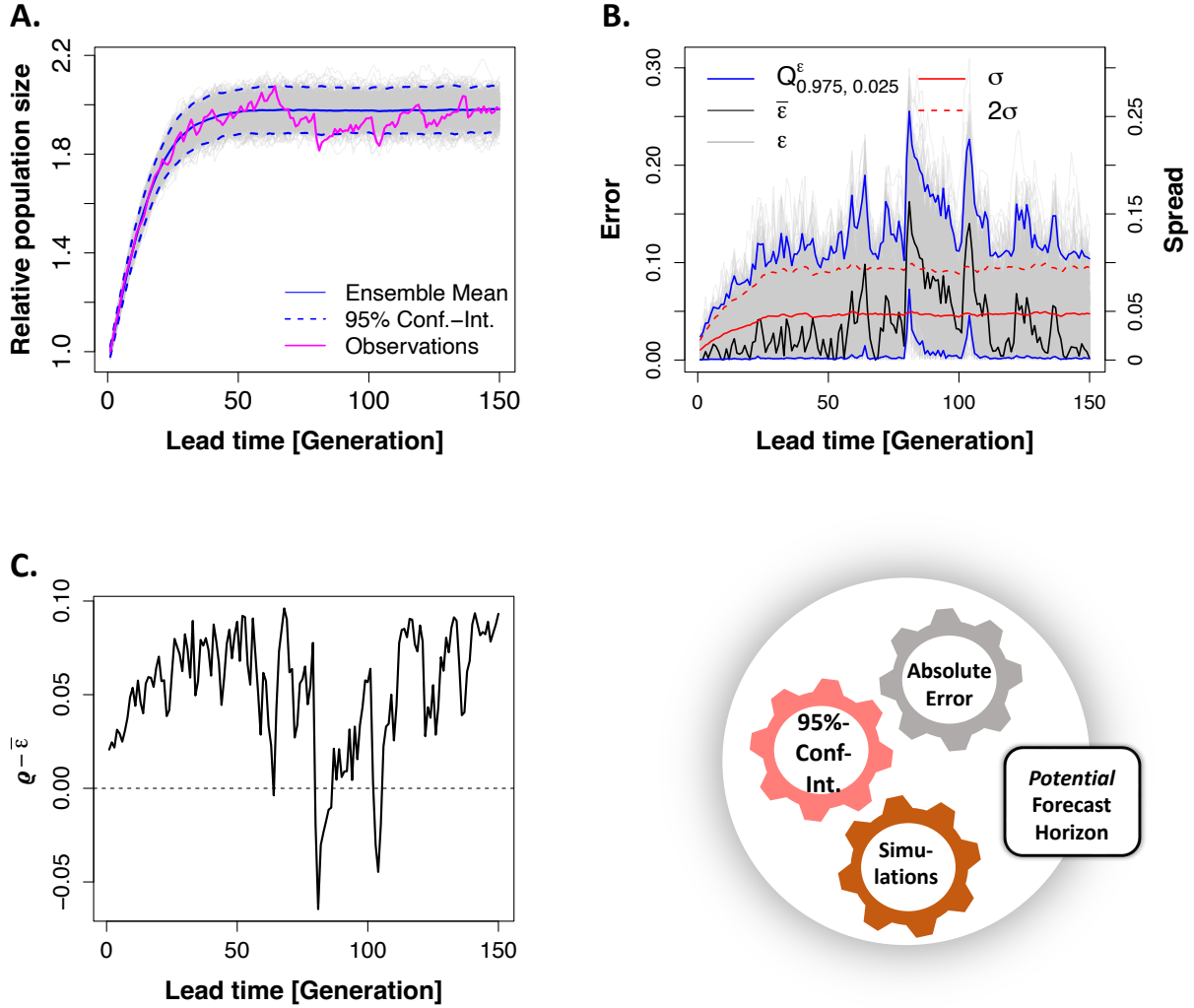


Figure 2: The forecast horizon in a case study with the stochastic Ricker model. **A.** Generational lead time evolution of the forecast distribution for relative population sizes, considering initial condition uncertainty and stochastic parameters. The solid blue lines indicates the ensemble mean and the dashed blue lines the 95% confidence interval of the ensemble forecast distribution. The pink line are the simulated observations. **B.** Ensemble errors and spread. Error are computed as absolute errors toward observations. We display ensemble member errors and quantiles (ϵ and Q respectively). The solid black line is the mean of ensemble member errors $\bar{\epsilon}$. The solid and dashed red lines indicate the ensemble spread with σ being the sample estimate of the ensemble standard deviation, and 2σ the confidence interval of the ensemble mean. **C.** The *potential* forecast horizon is reached as the mean ensemble error $\bar{\epsilon}$ exceeds ρ that is here the 95% confidence interval, i.e. as the solid black line drops below 0.

4.2 Chaotic Coupled Ricker model and the potential forecast horizon

Setting The forecast model $\mathcal{M}(Y_0, X, \theta)$ consists of two extended coupled Ricker-type (C-Ricker) equations, simulating a system with two populations as state variable \hat{Y} that constitutes the smallest unit of an ecosystem [59, 60]. We simulate a point process with seasonality-mimicking external forcing X and parameters θ that cause internally unstable behaviour, i.e. are set in a nearly chaotic regime. Population dynamics hence exhibit overcompensatory behavior that is specifically visible over temporal ranges with strong external influences, making the dynamics driven partly by external factors and partly by internal mechanisms (for model details, see Appendix).

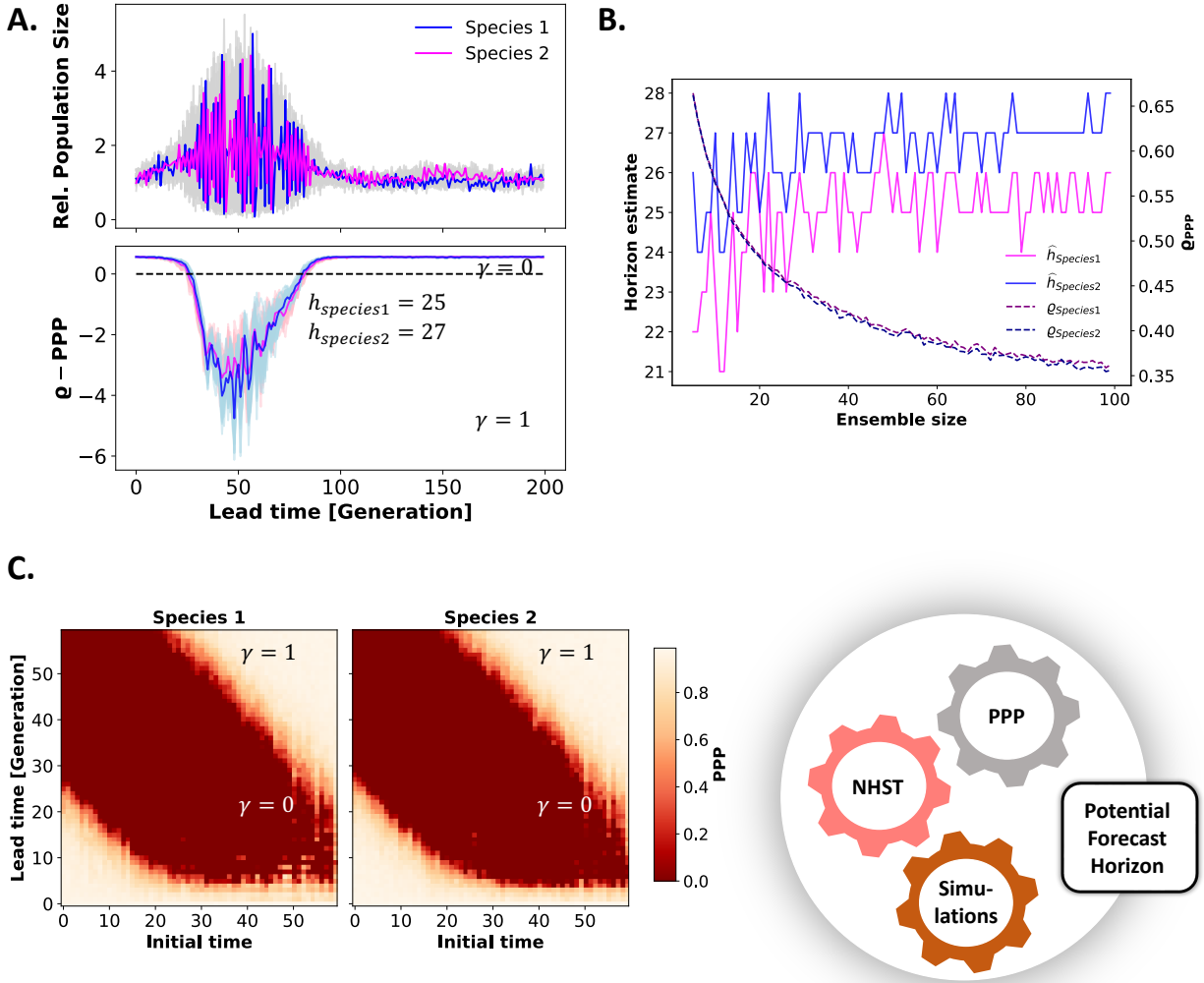


Figure 3: Potential forecast horizons of relative population sizes, estimated for a coupled Ricker model. **A.** Top: The observed climatology (in lightgray) and the observed population trajectories and which we forecast in a perfect-model ensemble framework. Bottom: Step wise computed potential prognostic predictability. The shaded areas indicate the uncertainty quantified by re-sampling from the forecast ensemble. **B.** The determined threshold ϱ_{PPP} and the subsequent forecast horizon as a function of ensemble size. **C.** Forecast horizons from varying initialisation. Vertical pattern indicate limits to initial conditions predictability. Diagonal pattern indicate dependence on seasonality. The system is estimated to be predictable at $g(t) = 1$ and unpredictable otherwise.

Potential forecast horizon Scoring function \mathcal{S} is the Potential Prognostic Predictability (PPP) (see equation 13) [44] that we compute independently for species 1 and 2. We forecast an ensemble of 50 trajectories with initial conditions drawn from a Gaussian distribution with a variance of 10% of initial size [46]. Uncertainty of the PPP is quantified by drawing 40 sub-samples with 80% of ensemble members. We test for differences in variances with an F-test at a significance level of $\alpha = 0.05$. Auto-correlation coefficients were $\gamma_1 = -0.47$ and $\gamma_2 = -0.43$ for species 1 and 2 respectively, yielding F-values as tolerances $\varrho_1 = 0.42$ and $\varrho_2 = 0.4$.

Results Potential forecast horizons were reached after 25 generations for species 1 and 27 generations for species 2 (figure 3, panel A). While the threshold ϱ strongly depends on the number of ensemble trajectories, this affects estimates of the potential forecast horizon only at small ensemble sizes (figure 3, panel B). Sequentially computed Lyapunov

exponents (see Appendix) range from -0.42 to -0.34 and their negative value indicates an overall stable dynamics, i.e. non-chaotic behaviour [61]. Nevertheless, varying the initial forecast time over the seasonal cycle showed that the limit of potential predictability is consistently reached after fewer than ten generations as the system approaches the region of overcompensation (figure 3, panel C).

4.3 Forest growth with iLand and the actual forecast horizon

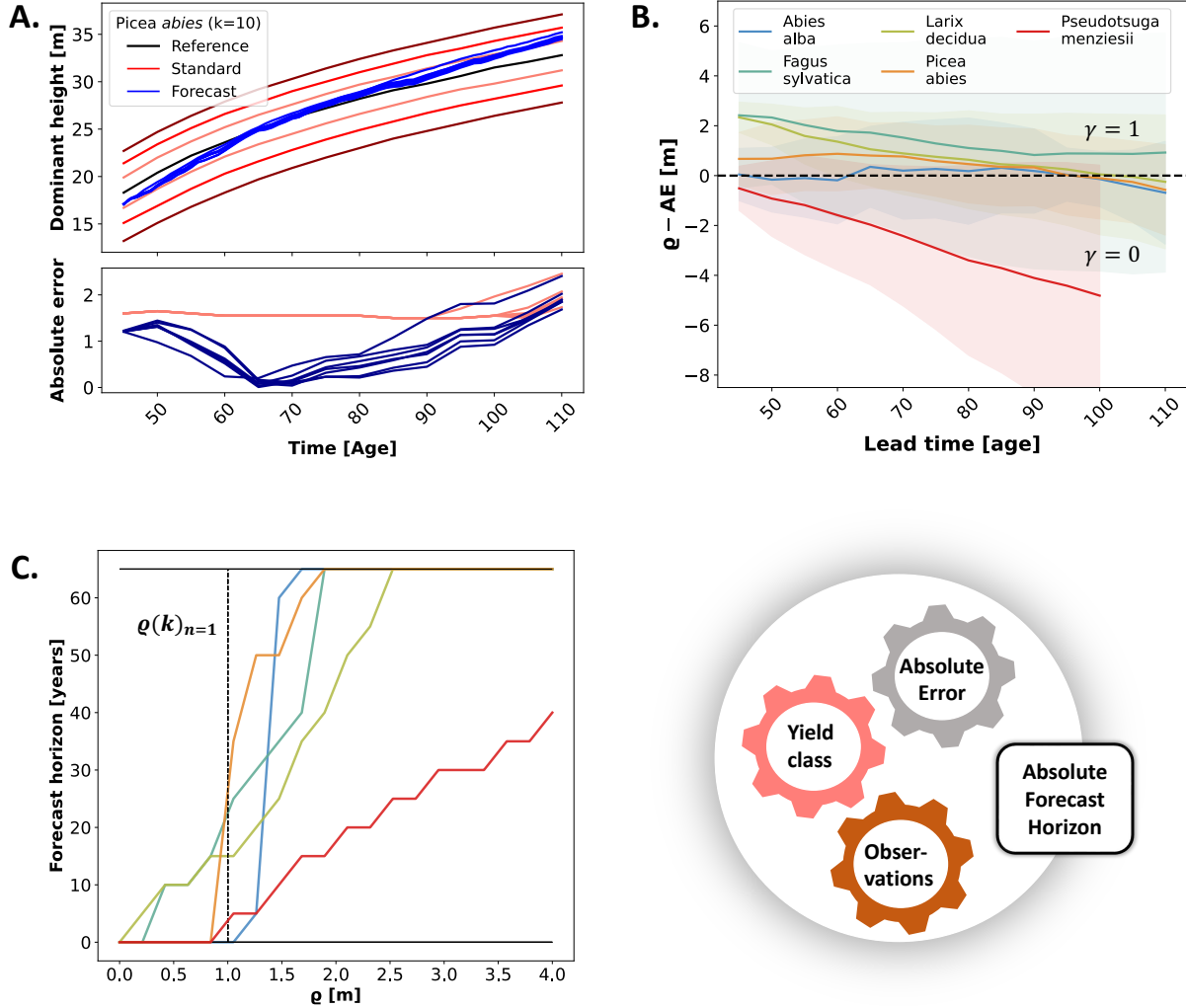


Figure 4: Actual forecast horizons for the dominant height of five tree species, forecasted with iLand. **A.** Top: Exemplary growth trajectories of the *Picea abies* stands of observed yield classes $k = 10$. Bottom: Error tolerances (red) toward the absolute forecast error by conditions toward neighbouring yield classes. **C.** Forecast horizons for all species that is reached when the mean trajectories drop below 0. Trajectories are aggregated over stands, shaded areas hence indicate the 95% confidence interval due to spatial variability. **B.** The forecast horizon as a function of the error tolerance ϱ (see [16]), independent of yield classes. The maximally possible horizon is 65 years, referring to the maximum simulated stand age of 110.

Setting The forecast model $\mathcal{M}(Y_0, X, \theta)$ is the individual-based forest landscape and disturbance model iLand [13, 62], which we use to demonstrate the actual forecast horizon of tree productivity. Primary tree productivity in iLand is represented for example by the stand dominant height (in meters), which we define as the system state \hat{Y} . Dynamics

of \widehat{Y} over time represents the stand age (in years). The process is forced on daily resolution by four meteorological variables X (temperature, precipitation, radiation and vapor pressure deficit). Soil and carbon parameters are treated as global parameters θ , being constant in time and space. Study area is the Freiburger Stadtwald that encompasses 269 sites and five tree species with varying numbers of observations. The forecasts are spatially aggregated by species over the stands. As reference Y , we used observations of dominant stand height as reconstructed from one-time forest inventory data and the dominant height growth described in regional yield tables for individual yield classes.

Actual forecast horizon We estimate the expected lower boundary of iLand’s forest horizon. Scoring function \mathcal{S} is the absolute error (AE) that collapses to the mean absolute error when spatially aggregated (see equation 11). In contrast to the previous case study, the scoring tolerance ϱ is set ad-hoc by the expected yield of an neighboring yield classes: ϱ is exceeded as the forecasted stand productivity changes from the observed to an adjacent yield class. This makes ϱ a function of the observed yield class k and the tolerated distance to neighboring yield classes n such that $\varrho(k)_{n=1}$ for a distance of one yield class (see figure 4, panel A). Consequently, $\varrho(k)_{n=1}$ varies among stands and species.

Results iLand’s actual forecast horizons varied notably both among and within species (see Figure 4, Panel B). With our strict definition of $n = 1$, average horizons were not longer than 75 years in stand age for *Picea abies*, which corresponded to 35 years into the simulation; *Pseudotsuga menziesii* even showed an average horizon at stand age 45 corresponding to 0 years into the simulation. Yet, horizons varied strongly among stands and were specifically long for *Picea abies* and *Fagus sylvatica*, where some stands show horizons until the maximum lead time. Showing the forecast horizon as a function of the absolute error tolerance ϱ (see Figure 4, Panel C) is equivalent to shifting the dashed line in Panel B up or down. It reveals that a tolerance with two neighboring yield classes, $\varrho(k)_{n=2}$, would extend the forecast horizon of three species to the full lead time of 110 years.

4.4 Land surface emulation and the relative forecast horizon

Setting The forecast model $\mathcal{M}(Y_0, X, \theta)$ is a model-ensemble-based machine learning emulator of ECMWF’s physical land surface scheme ecLand (hereafter: aiLand) [47, 9] which we use to demonstrate both absolute and relative forecast horizons [27]. aiLand consists of three sub-models: A feed forward neural network, a long short-term memory neural network and an extreme gradient boosting algorithm [9]. State variables \widehat{Y} of the model-ensemble are soil water volume (m^3m^{-3}) and soil temperature (K) at the soil surface layer (0-5 cm), subsurface layer 1 (5-20 cm) and subsurface layer 2 (20-70 cm), and snow cover. All states together initialise \mathcal{M} as Y_0 . External processes X that force Y are ERA-5 reanalysis dynamic meteorological variables and static climate and physiographic fields [63]. The details on model and variables are described in [9]. We show our analysis for soil temperature. aiLand is evaluated on observations from the International Soil Moisture Network (ISMN) that provides a quality-controlled and harmonised data base for land-surface process evaluation [64]. We use local observations from years 2021 and 2022 of $m = 13$ French Smosmania network stations, that we define as the reference \mathbf{Y} . Soil temperature was measured at 0-5 cm (surface layer), 5-20 cm (subsurface layer 1) and 20-30 cm (subsurface layer 2). aiLand is exemplarily initialised with observations on February 1st 2022, constituting initial conditions Y_0 , and is then integrated at a 6-hourly temporal resolution over $\tau = 1, \dots, 56$ lead times, representing the medium-range. For long-range forecasts $\tau = 1, \dots, 1200$ and soil water volume results, see Appendix.

Actual and relative forecast horizons We compute an absolute and a relative forecast horizon of aiLand. Scoring function \mathcal{S} is the mean absolute error (MAE) and the ad-hoc scoring tolerance for soil temperature is $\varrho = 1.5K$ [39]. The relative forecast horizon is determined by computing aiLand skill toward the numerical ecLand as null model, as such \mathcal{S} becomes the MAE-SS, a first order skill scoring function [58]. The MAE is spatially averaged over stations and, considering aiLand is as a model-ensemble, can be computed as

$$\text{MAE}_{\text{aiLand}_t} = \frac{1}{m} \sum |\widehat{Y}_t - \mathbf{Y}_{t,m}|, \quad \text{where } m = 1, \dots, 13 \quad \text{and } t = 1, \dots, \tau \quad (15)$$

where \widehat{Y}_m is the model-ensemble mean. Skill is hence stepwise evaluated as

$$\text{MAE-SS}_t = 1 - \frac{\text{MAE}_{\text{aiLand}}(\widehat{Y}_t, \mathbf{Y}_{t,m})}{\text{AE}_{\text{ecLand}}(\widehat{Y}_t, \mathbf{Y}_{t,m})}, \quad \text{where } t = 1, \dots, \tau, \quad (16)$$

and where the MAE step-wise averages over the emulator model-ensemble, but in fact, for only one station reduces the point forecast of physical ecLand to a point-wise absolute error.

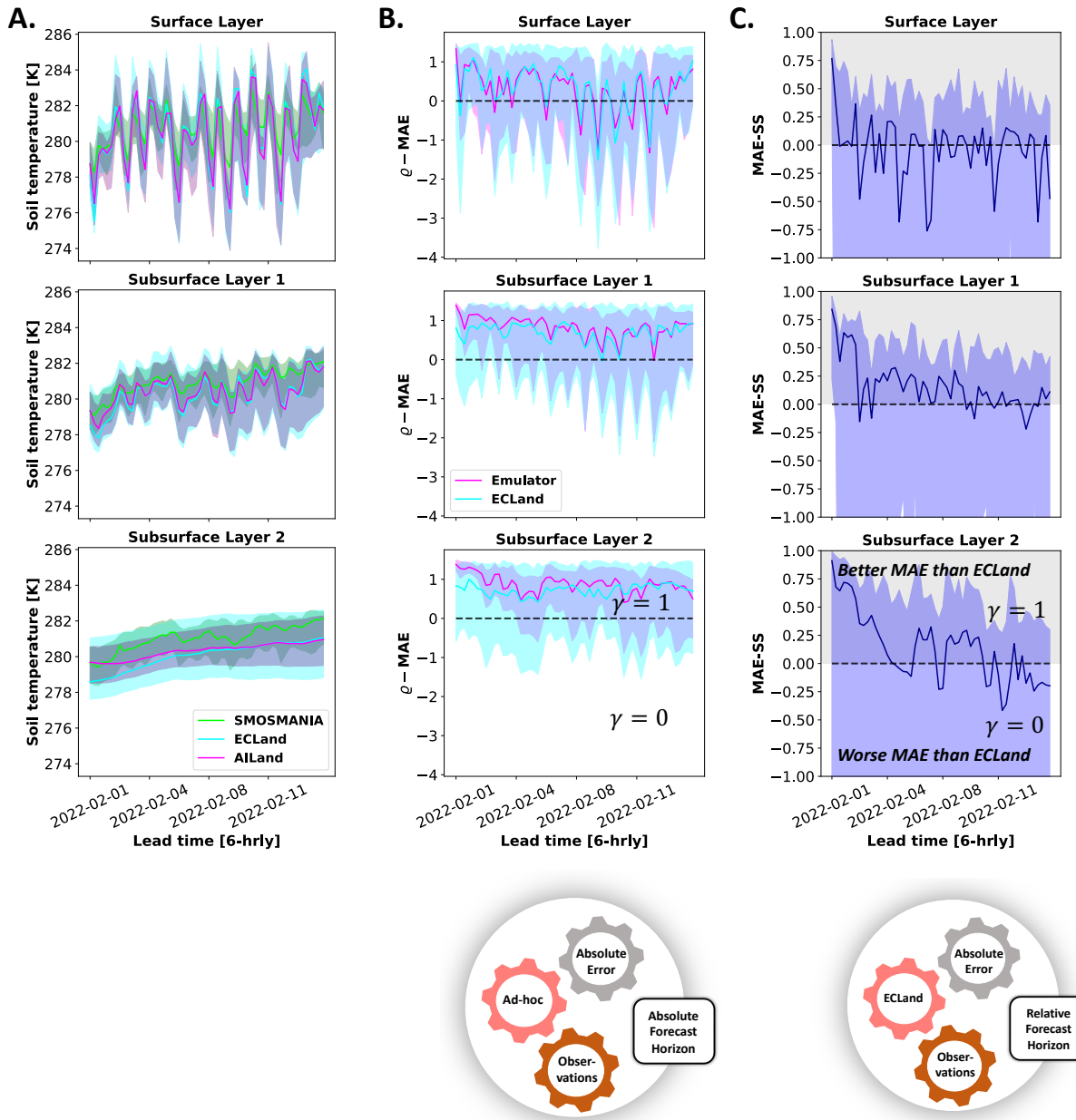


Figure 5: **A.** Forecast of aiLand and of numerical ecLand for soil temperature measurements across Smosmania (F) stations at the surface and two subsurface layers over a medium-range test period in February 2022. **B.** Actual forecast horizons of aiLand and ecLand with a tolerance of 1.5 K toward the predictive MAE on the Smosmania station measurements. **C.** Relative forecast horizon based on the MAE-SS of aiLand toward ecLand. Gray shaded regions indicate areas where the MAE of aiLand is smaller than that of ecLand.

Results We found a general agreement in station data and average model forecasts (see figure 5, Panel A). Models exhibited a diurnal pattern over the medium-range on the surface layer that attenuated toward deeper layers. At an error tolerance of 1.5 K, ecLand and aiLand show similar and lower average predictability at the surface layer than in the subsurface layers. ecLand has higher spatial variability than aiLand (Panel B). Initialised with observations, aiLand has an advantage over non-initialised ecLand at short lead times (Panel C and figure 6): The relative forecast horizon of aiLand is 12 hours on the surface layer, nearly two days on subsurface layer 1 and 4 days on subsurface layer 2. After this time period, the information from the observations seems to vanish and aiLand approaches the physical model again.

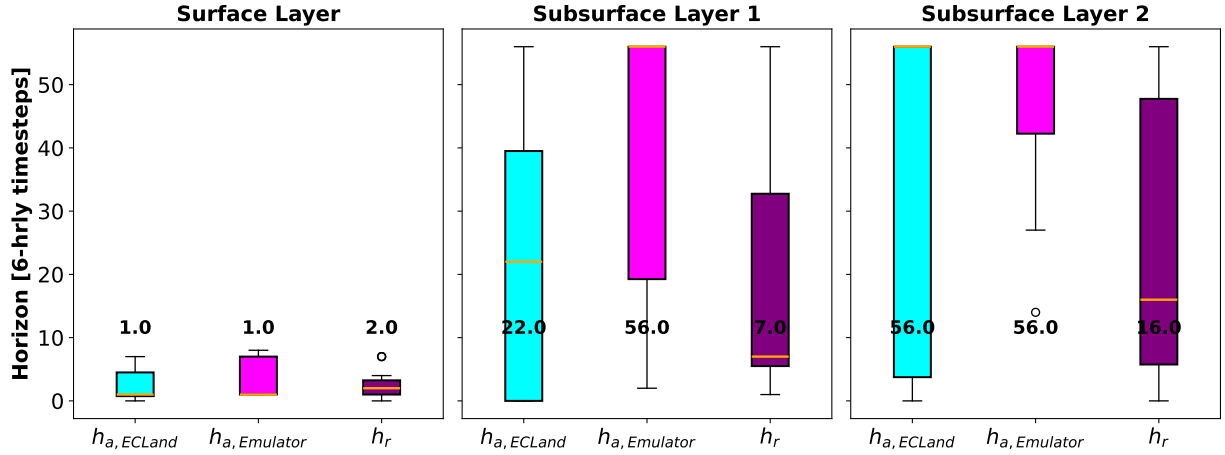


Figure 6: The actual (h_a) and relative (h_r) empirical forecast horizons computed for ecLand and aiLand at three different soil layers. Variability in the box plots refers to variability over network stations. The median horizons (orange) indicate an increasing predictability towards lower layers. A positive h_r indicates the horizons up to which aiLands initialization with observations shows more skill than ecLand.

5 Discussion

Our intention is to highlight the relevance of quantified forecast horizons and improve the credibility when communicating model-based forecasts. We motivated, distinguished and demonstrated three ways of determining empirical forecast horizons that we termed potential, actual and relative forecast horizon.

5.1 Motivating forecast horizons

Mechanistic statements about random processes will always include errors [65] and ideally, forecasts make statements about the future with full uncertainty propagation [22, 23]. While we did not propagate all sources uncertainties in simultaneously in any of our case studies, we address them across studies: In our motivational study with the stochastic Ricker model, we illustrate the forecast horizon with parameter uncertainty propagation. In our case study with the chaotic Ricker model, we assess the potential forecast horizon with initial conditions uncertainty. In our case study with iLand, we consider the impact of forcing variability on the actual forecast horizon through spatial aggregation. In our case study with ecLand, we address model structural uncertainty by evaluating aiLand as a model-ensemble and forcing variability by spatial aggregation.

The predictability of any stochastic Markov system declined over time [52], when predictability was defined based on the dispersion of the forecast distribution, i.e. the noise or spread [50]. This finding assumes that more spread in the distribution will lead to larger predictive errors, i.e. a positive spread-error correlation. If this is the case for a specific predictability analysis depends on how we quantify spread and error, respectively [57]. Optimally, the demonstration of forecast horizons will be extended in future studies with full error propagation for each case study simultaneously and the respective spread-error correlation being assessed.

5.2 Potential, actual and relative horizons

Chaotic Ricker For the chaotic coupled Ricker model, we determined the potential upper forecast horizon. It is, however, system and model dependent if \hat{h}_p provides a good estimate of \hat{h} . The seasonality in the simulation causes predictability to rebound at long-range, but is limited at short-range forecasts [52]. The F-test relies on the parametric assumptions of homogeneity and independence of variances. These assumptions are partially met by the step-wise ensemble evaluation [42], yet for computing the total climatological variance we aggregate over overcompensation areas. This explains the strong decline in PPP in this range and may lead to a small effect of ensemble size on the computed horizons, while ϱ_{PPP} , derived assuming an F-distribution with degrees of freedom as parameters, strongly depends on it. \hat{h}_p may further depend on model parameter uncertainty. We explored horizon sensitivity to the hyper-parameters initialisation time and ensemble size, yet sensitivities of population growth rates and seasonality-modulating parameters could be explored in a global sensitivity analysis [66, 67].

iLand Stand productivity in iLand is a stable state variable and its absolute forecast horizon is determined by external standards. While this approach implicitly introduces forecast utility [34], in evaluation we focus on forecast quality and therefore the technical limitations. iLand is commonly used for projections, but the empirical framework we employ requires reference data to determine forecast accuracy. Ideally, observational data would serve as the primary reference. However, with only three inventory measurements per stand over a 30-year span, we relied on reconstructed observations from yield tables as the most viable alternative, which, strictly speaking, are also model-based (see description in the Appendix, Case Study 2); thus, this analysis cannot be used to draw definitive conclusions about iLand, but serves as a demonstration of specifying predictive error tolerance based on available standards.

ecLand We demonstrate actual and relative forecast horizons (\hat{h}_a, \hat{h}_r) of an ensemble of ecLand emulators, aiLand, on the medium-range, testing suitability for weather forecasting. With an scoring tolerance of 1.5 Kelvin we compute \hat{h}_a : the horizon up to which aiLand has an acceptable error magnitude for stable modeling of land-atmosphere interactions [47, 39]. We explore whether the flexibility to quickly initialise prognostic states may be an advantage of aiLand over the physical model. As such, ecLand was not initialised with observations, but aiLand was. The horizon up to which this advantage is detectable is indicated by the positive \hat{h}_r , which extends towards lower soil layers. This can be interpreted as an increasing memory for initialisation for slower variables, which is even more visible for soil moisture (see Appendix). The \hat{h}_r could potentially be further extended by fine-tuning aiLand on station data. Forecast errors arise not only because of model structures but also due to uncertainty in meteorological forcing: The models forecast to a 31 km spatial grid, while observations are local measurements. As such, when ecLand and aiLand are both driven by erroneous forcing, neither can be expected to have a long \hat{h}_a . We show only a local excerpt from aiLand's capabilities by looking at horizons from a single initialisation time and for soil temperature only. For completeness, we extended the analysis also to the subseasonal range, but without additional results (see Appendix). To better assess predictive ability, the effect of initialisation period on the forecast horizons can be explored over the full yearly cycle as in [9]. Further, soil temperature interacts strongly with soil moisture and their horizons are likely not independent. We did a first analysis on soil moisture horizons (preliminary results in Appendix). However, the same analysis for soil moisture is non-trivial due to its different definitions based on soil type.

5.3 Forecast horizons beyond chaotic systems

The forecast horizon was originally defined for sub-seasonal weather forecasting of the endogenously unstable system of the atmosphere [68]. Instability of a system puts an upper bound its predictability and is caused by sensitivity to initial conditions, which can lead to exponential growth of predictive errors [54, 35]. Unstable dynamics may exist in natural populations [61], but many ecosystems are assumed to exist in alternative stable states [69]. As open systems, ecosystems are externally driven by meteorological forcing [70]. This is also well known for hydrological forecasts, which, being driven by medium-range weather forcing, have an estimated predictability horizon of 10 to 14 days [71, 72]. Land-surface predictability is limited by seasonality, hence strongly location-dependent [73, 72]. In seasonal forecasting with strong boundary conditions, a forecast horizon is only reached temporarily in areas of low predictability. In coupling to atmospheric models, this phenomenon has been called ‘the return of skill’ [52], which is most clearly visible in our second case study. While recent insights suggest sensitivity to initial conditions in decadal forecasting of forest ecosystems [74], we do not explore how initial conditions uncertainty affects actual horizons of iLand or ecLand. However, a full predictability analysis for these case studies is of interest, where one would also explore the potential forecast horizon by perturbing initial state variables.

5.4 Contributions to ecological forecasting

Box 1. DIY empirical forecast horizons.

To encourage their computation, we give a recipe on how to compute a forecast horizon of a forecasting model \mathcal{M} within your experiment. To pick an approach that suits your experimental setting, follow the decision tree in figure 7, which suggests starting points for the choices we illustrated.

Step 1: Select your reference. In a hindcasting setting, these are observations Y . If no observational reference is available, compute Y as mean trajectory of the perturbation ensemble for the potential forecast horizon (at step 3).

Step 2: Select scoring function(s). You need one or more functions \mathcal{S} that quantify forecast error, spread and/or skill.

Step 3 (h-dependent): Specify error tolerance. For the actual forecast horizon, specify an error tolerance ϱ . This is a requirement for applying forecast horizons, and often available as system knowledge. Alternatively, provide ad-hoc tolerances based on ecological reasoning, e.g. as percentage in the unit of the state variable (e.g. [20, 65]).

Step 4 (h-dependent): Propagate uncertainties. If reference are model simulations, error propagation is necessary. For the potential forecast horizon, propagate initial states perturbation, for parametric uncertainty using, e.g., Monte Carlo sampling techniques.

Step 5: Make forecast. Run your forecast model to compute $\hat{Y}^{\mathcal{M}}$. For the relative forecast horizon, use your benchmark or null model \mathcal{M} to create $\hat{Y}^{\mathcal{R}}$.

Step 6: Step-wise evaluation. Quantify forecast error, spread and/or skill step-wise over time with the scoring function \mathcal{S} .

Step 7: Determine horizon. Test, if score is exceeding the pre-defined error tolerance ϱ by step-wise evaluating the condition $\varrho - \mathcal{S} < 0$.

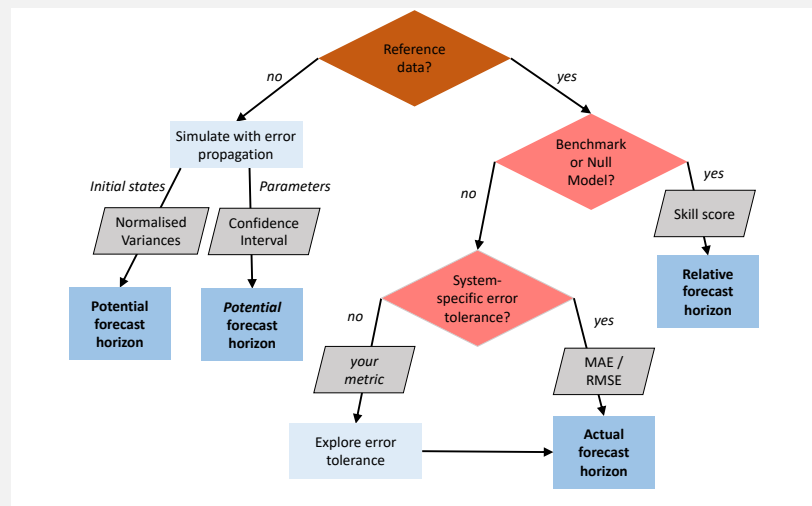


Figure 7: Decision tree for horizon approaches. Diamonds check the availability of ingredients required for the respective horizon. We suggest a selection of scoring function for a start.

We propose establishing forecast horizons to monitor ecological forecasting systems and enhance the tractability of model-based statements in ecology for both the scientific community and decision-makers [22]. Forecast horizons enable tracking the skill development of forecasting systems [75]. They establish objective, quantitative assessments of forecast skill at various lead times, and we can use them to conduct systematic benchmarking and identify paradigm shifts or significant advancements in ecological forecasting. Based on the previous state of discussion on empirical forecast horizons [20], we identified three dimensions for their computation: the scoring function, the evaluation reference, and the predictive error tolerance (ϱ). We extended previous works elaborating the dimensions in a formal framework. Based on their combinations, we differentiated three types of studying empirical limits of system predictability and model predictive ability that we categorised as potential, actual and relative forecast horizon [44, 42, 55, 27]: The potential forecast horizon assesses the internal predictability of the modeled system. It is the horizons upper boundary estimate, conditional on the model, and applicable without data or specifying an ad-hoc predictive error tolerance. The actual forecast horizon assesses the predictive ability by evaluation with observations. It is applicable by ad-hoc specifying a tolerance towards the predictive error. The relative forecast horizon assesses predictive ability compared to a benchmark model. It is useful for model comparisons of any type, as we demonstrated with the case of initialising aiLand with observations.

5.5 Directions from here

To facilitate comparison across ecological forecasting studies, we suggest a range scoring functions when reporting forecast horizons with deterministic evaluation [76]. Traditionally assessed with the signal-to-noise ratio [73], the

upper boundary of system predictability, the potential forecast horizon, can be assessed with the Potential Prognostic Predictability (PPP) [44]. For quantifying a model’s actual predictive ability, RMSE and MAE are well known and interpretable scores that assess the arithmetic mean and median of predictive errors, respectively [56]. The skill scores can be computed in comparison to a benchmark model and assess the relative forecast horizon. Any of these yield sample-based estimators that are accordingly sample size dependent [57]. Our approaches in this work concentrated mainly on evaluation of deterministic forecasts, while in ensemble forecasting it is also important to consider the spread-error relationship. This relationship is defined as the correlation between forecast error of the ensemble mean and the ensemble spread [57]. This relationship is used in ensemble forecasting to assess the reliability of predictions and it measures how well the ensemble spread reflects forecast uncertainty: A strong correlation between spread and error indicates that the model ensemble can reliably estimate forecast uncertainty. We demonstrate ensemble spread and mean ensemble error in our motivating case study, because under normal assumptions their relation represents if observations can be found within the 95% confidence interval (see figure 2). However, by incorporating this relationship deeper into the evaluation of forecast skill horizons, particularly in ensemble-based models like aiLand, we can provide a more robust assessment of model reliability. Future work could apply spread-error metrics, such as the mean squared error versus ensemble spread, to enhance the evaluation of forecast skill across different time horizons.

5.6 Limitations

We explored the choices of the three dimensions (scoring, reference, ρ ; see figure 1) in mainly a static algorithmic setup for computing different forecast horizons. However, an empirical forecast horizon is influenced by various sources of uncertainty that affect model and forecast accuracy and hence ε : model fit, including parameter sensitivity, ensemble size, and initial condition uncertainty. Similar to what has been done before in exploration of the horizon sensitivity to the cut-off value in [16], a full predictability assessment would involve disentangling these sources of ε [48, 74]. Consequently, we want to stress that the forecast horizons we compute are conditional on the respective model \mathcal{M} (see 1) and thus they do not represent the “true” limits of predictability. The potential forecast horizon may be a good estimate of the actual forecast horizon, but this is system specific [36]: How well does \mathcal{M} capture the features of the system? Further, if a different model was used to forecast the same process, we are likely to find a different estimate for the horizon [77]. Model-ensembles such as the land surface emulator can be used to account for model structural uncertainty [78]. The forecast horizon only makes sense under the same conditions forecasting does: permanence of the system. A meteorite strike will make all forecasting obsolete.

6 Conclusion

The forecast horizon can be defined and applied for practically any ecological forecast, as we demonstrated from theoretical to applied cases. Their empirical computation based on scoring functions always requires a reference, be it observations or model simulations. Choices of the scoring function, the reference and the error tolerance lead to different types of forecast horizons (actual, relative, potential). We suggest that ecological and indeed environmental forecasts should be accompanied by computations of forecast horizons to facilitate interpretation and communication. Future studies will have to evaluate which choices should be recommended; for now any of these combinations can be seen as a complementing information to the forecast itself. In summary, the demonstrated concepts may best be simultaneously applied and extended to establish a field of ecological predictability analysis. We gave outlines on how to continue research and underlined this with specific case studies. It could be impactful to demonstrate the relevance of forecast horizons at more recent examples with many data, or more complex ecological systems such as in [79, 16]. Yet, our case studies represent relevant scenarios with models that are used in operational forecasting (Emulator), models that are used for decision making (iLand) in a field where predictive ecology is already practiced successfully [80] and models that are used to explore hypotheses qualitatively and theoretically (Ricker) [65].

Code and Data availability

ISMN data is available under the following link: <https://ismn.earth/en/>. Data for iLand simulations is currently only available on request. Code for the analysis is published at: <https://github.com/MWesselkamp/forecast-horizons>.

Author Contributions

MW, FP and CD conceived the study. MW and JA conducted the analysis. MW and WJC wrote the formalisation. EP provided comments and evaluation data bases. FP and WJC reviewed the study. MW, JA, FP and CD wrote the manuscript.

Acknowledgments

This work profitted from helpful discussions with Souhail Boussetta, Christoph Rüdiger, Gabriel Moldovan and Hannah Habenicht. We gratefully thank Margarita Choulga and David Fairbairn for providing pre-processed ISMN data, and the FVA-BW for the BW-Inventory Data. We thank ECMWF for computational resources, ERA5 data and climate fields, and financial support for the research visits of MW. CD acknowledges partial funding by DFG CRC 1537 Ecosense.

References

- [1] Sydne Record, Carl Boettiger, and Christine R. Rollinson. Synthesizing forecasts to inform decision-making and advance ecological theory. *Methods in Ecology and Evolution*, 14(3):728–731, March 2023.
- [2] Ecological Forecasting Initiative. Ecological Forecasting Initiative Newsletter, July 2024.
- [3] Ryan Keisler. Forecasting global weather with graph neural networks, February 2022. arXiv:2202.07575 [physics].
- [4] Peter Bauer, Peter Dueben, Matthew Chantry, Francisco Doblas-Reyes, Torsten Hoefler, Amy McGovern, and Bjorn Stevens. Deep learning and a changing economy in weather and climate prediction. *Nature Reviews Earth & Environment*, 4(8):507–509, August 2023.
- [5] Zied Ben Bouallègue, Mariana C. A. Clare, Linus Magnusson, Estibaliz Gascón, Michael Maier-Gerber, Martin Janoušek, Mark Rodwell, Florian Pinault, Jesper S. Dramsch, Simon T. K. Lang, Baudouin Raoult, Florence Rabier, Matthieu Chevallier, Irina Sandu, Peter Dueben, Matthew Chantry, and Florian Pappenberger. The rise of data-driven weather forecasting: A first statistical assessment of machine learning–based weather forecasts in an operational-like context. *Bulletin of the American Meteorological Society*, 105(6):E864–E883, June 2024.
- [6] Jacob A. Zwart, Samantha K. Oliver, William David Watkins, Jeffrey M. Sadler, Alison P. Appling, Hayley R. Corson-Dosch, Xiaowei Jia, Vipin Kumar, and Jordan S. Read. Near-term forecasts of stream temperature using deep learning and data assimilation in support of management decisions. *JAWRA Journal of the American Water Resources Association*, 59(2):317–337, April 2023.
- [7] Grey Nearing, Deborah Cohen, Vusumuzi Dube, Martin Gauch, Oren Gilon, Shaun Harrigan, Avinatan Hassidim, Daniel Klotz, Frederik Kratzert, Asher Metzger, Sella Nevo, Florian Pappenberger, Christel Prudhomme, Guy Shalev, Shlomo Shenzenis, Tadele Yednkachw Tekalign, Dana Weitzner, and Yossi Matias. Global prediction of extreme floods in ungauged watersheds. *Nature*, 627(8004):559–563, March 2024.
- [8] Wayne M. Getz, Charles R. Marshall, Colin J. Carlson, Luca Giuggioli, Sadie J. Ryan, Stephanie S. Romañach, Carl Boettiger, Samuel D. Chamberlain, Laurel Larsen, Paolo D’Odorico, and David O’Sullivan. Making ecological models adequate. *Ecology Letters*, 21(2):153–166, February 2018.
- [9] Marieke Wesselkamp, Matthew Chantry, Ewan Pinnington, Margarita Choulga, Souhail Boussetta, Maria Kalweit, Joschka Bödecker, Carsten F. Dormann, Florian Pappenberger, and Gianpaolo Balsamo. Advances in land surface model-based forecasting: A comparison of LSTM, Gradient Boosting, and feedforward neural networks as prognostic state emulators in a case study with ECLand, August 2024.
- [10] Uriah Daugaard, Stephan B. Munch, David Inauen, Frank Pennekamp, and Owen L. Petchey. Forecasting in the face of ecological complexity: Number and strength of species interactions determine forecast skill in ecological communities. *Ecology Letters*, 25(9):1974–1985, September 2022.
- [11] K.A.N.K. Karunarathna, Konstans Wells, and Nicholas J. Clark. Modelling nonlinear responses of a desert rodent species to environmental change with hierarchical dynamic generalized additive models. *Ecological Modelling*, 490:110648, April 2024.
- [12] Marko Kazimirović, Branko Stajić, Nenad Petrović, Janko Ljubičić, Olivera Košanin, Marc Hanewinkel, and Dominik Sperlich. Dynamic height growth models for highly productive pedunculate oak (*Quercus robur* L.) stands: explicit mapping of site index classification in Serbia. *Annals of Forest Science*, 81(1):15, March 2024.
- [13] Rupert Seidl, Werner Rammer, Robert M. Scheller, and Thomas A. Spies. An individual-based process model to simulate landscape-scale forest ecosystem dynamics. *Ecological Modelling*, 231:87–100, April 2012.
- [14] R. Quinn Thomas, Renato J. Figueiredo, Vahid Daneshmand, Bethany J. Bookout, Laura K. Puckett, and Cayelan C. Carey. A near-term iterative forecasting system successfully predicts reservoir hydrodynamics and partitions uncertainty in real time. *Water Resources Research*, 56(11), November 2020.
- [15] Abigail S. L. Lewis, Christine R. Rollinson, Andrew J. Allyn, Jaime Ashander, Stephanie Brodie, Cole B. Brookson, Elyssa Collins, Michael C. Dietze, Amanda S. Gallinat, Noel Juvigny-Khenafou, Gerbrand Koren, Daniel J. McGlenn, Hassan Moustahfid, Jody A. Peters, Nicholas R. Record, Caleb J. Robbins, Jonathan Tonkin,

- and Glenda M. Wardle. The power of forecasts to advance ecological theory. *Methods in Ecology and Evolution*, pages 2041–210X.13955, August 2022.
- [16] Elias C. Massoud, Jef Huisman, Elisa Benincà, Michael C. Dietze, Willem Bouten, and Jasper A. Vrugt. Probing the limits of predictability: data assimilation of chaotic dynamics in complex food webs. *Ecology Letters*, 21(1):93–103, January 2018.
- [17] Hamze Dokoohaki, Bailey D. Morrison, Ann Raiho, Shawn P. Serbin, Katie Zarada, Luke Dramko, and Michael Dietze. Development of an open-source regional data assimilation system in PEcAn v. 1.7.2: application to carbon cycle reanalysis across the contiguous US using SIPNET. *Geoscientific Model Development*, 15(8):3233–3252, April 2022.
- [18] Michael C. Dietze, Andrew Fox, Lindsay M. Beck-Johnson, Julio L. Betancourt, Mevin B. Hooten, Catherine S. Jarnevich, Timothy H. Keitt, Melissa A. Kenney, Christine M. Laney, Laurel G. Larsen, Henry W. Loescher, Claire K. Lunch, Bryan C. Pijanowski, James T. Randerson, Emily K. Read, Andrew T. Tredennick, Rodrigo Vargas, Kathleen C. Weathers, and Ethan P. White. Iterative near-term ecological forecasting: Needs, opportunities, and challenges. *Proceedings of the National Academy of Sciences*, 115(7):1424–1432, February 2018.
- [19] Michael C. Dietze, R. Quinn Thomas, Jody Peters, Carl Boettiger, Gerbrand Koren, Alexey N. Shiklomanov, and Jaime Ashander. A community convention for ecological forecasting: Output files and metadata version 1.0. *Ecosphere*, 14(11):e4686, November 2023.
- [20] Owen L. Petchey, Mikael Pontarp, Thomas M. Massie, Sonia Kéfi, Arpat Ozgul, Maja Weilenmann, Gian Marco Palamara, Florian Altermatt, Blake Matthews, Jonathan M. Levine, Dylan Z. Childs, Brian J. McGill, Michael E. Schaepman, Bernhard Schmid, Piet Spaak, Andrew P. Beckerman, Frank Pennekamp, and Ian S. Pearse. The ecological forecast horizon, and examples of its uses and determinants. *Ecology Letters*, 18(7):597–611, July 2015.
- [21] Brett Raczka, Michael C. Dietze, Shawn P. Serbin, and Kenneth J. Davis. What Limits Predictive Certainty of Long-Term Carbon Uptake? *Journal of Geophysical Research: Biogeosciences*, 123(12):3570–3588, December 2018.
- [22] James S. Clark, Steven R. Carpenter, Mary Barber, Scott Collins, Andy Dobson, Jonathan A. Foley, David M. Lodge, Mercedes Pascual, Roger Pielke, William Pizer, Cathy Pringle, Walter V. Reid, Kenneth A. Rose, Osvaldo Sala, William H. Schlesinger, Diana H. Wall, and David Wear. Ecological forecasts: An emerging imperative. *Science*, 293(5530):657–660, July 2001.
- [23] Michael Christopher Dietze. *Ecological forecasting*. Princeton University Press, Princeton, 2017.
- [24] Blake A. Schaeffer, Natalie Reynolds, Hannah Ferriby, Wilson Salls, Deron Smith, John M. Johnston, and Mark Myer. Forecasting freshwater cyanobacterial harmful algal blooms for Sentinel-3 satellite resolved U.S. lakes and reservoirs. *Journal of Environmental Management*, 349:119518, January 2024.
- [25] Mark C Urban, Justin M J Travis, Damaris Zurell, Patrick L Thompson, Nicholas W Synes, Alice Scarpa, Pedro R Peres-Neto, Anne-Kathleen Malchow, Patrick M A James, Dominique Gravel, Luc De Meester, Calum Brown, Greta Bocedi, Cécile H Albert, Andrew Gonzalez, and Andrew P Hendry. Coding for life: Designing a platform for projecting and protecting global biodiversity. *BioScience*, 72(1):91–104, January 2022.
- [26] Susan Harrison, Andy Stahl, and Daniel Doak. Spatial Models and Spotted Owls: Exploring Some Biological Issues Behind Recent Events. *Conservation Biology*, 7(4):950–953, December 1993.
- [27] Roberto Buizza and Martin Leutbecher. The forecast skill horizon. *Quarterly Journal of the Royal Meteorological Society*, 141(693):3366–3382, October 2015.
- [28] Edward N. Lorenz. Deterministic Nonperiodic Flow. *Journal of the Atmospheric Sciences*, 20, January 1963.
- [29] Brian R. Hunt, Tien-Yien Li, Judy A. Kennedy, and Helena E. Nusse, editors. *The theory of chaotic attractors*. Springer New York, New York, NY, 2004.
- [30] Linus Magnusson, Jan-Huey Chen, Shian-Jiann Lin, Linjiong Zhou, and Xi Chen. Dependence on initial conditions versus model formulations for medium-range forecast error variations. *Quarterly Journal of the Royal Meteorological Society*, 145(722):2085–2100, July 2019.
- [31] Paolo Reggiani, Daniela Biondi, and Ezio Todini. On time-horizons based post-processing of flow forecasts. *Frontiers in Water*, 6:1359750, April 2024.
- [32] Peter B. Adler, Ethan P. White, and Michael H. Cortez. Matching the forecast horizon with the relevant spatial and temporal processes and data sources. *Ecography*, 43(11):1729–1739, November 2020.
- [33] Whitney M. Woelmer, R. Quinn Thomas, Mary E. Lofton, Ryan P. McClure, Heather L. Wander, and Cayelan C. Carey. Near-term phytoplankton forecasts reveal the effects of model time step and forecast horizon on predictability. *Ecological Applications*, 32(7), October 2022.

- [34] Allan H. Murphy. What is a good forecast? An essay on the nature of goodness in weather forecasting. *Weather and Forecasting*, 8(2):281–293, June 1993.
- [35] Amnon Dalcher and Eugenia Kalnay. Error growth and predictability in operational ECMWF forecasts. *Tellus A*, 39A(5):474–491, October 1987.
- [36] Timothy DelSole and Michael Tippett. *Statistical Methods for Climate Scientists*. Cambridge University Press, 1 edition, January 2022.
- [37] ECMWF. Forecast User Guide.
- [38] James C McWilliams. A perspective on the legacy of Edward Lorenz. *Earth and Space Science*, (6):336–350, December 2018.
- [39] Junzhi Zhou, Jiang Zhang, and Yuanyuan Huang. Evaluation of soil temperature in CMIP6 multimodel simulations. *Agricultural and Forest Meteorology*, 352:110039, June 2024.
- [40] F. Pappenberger, M.H. Ramos, H.L. Cloke, F. Wetterhall, L. Alfieri, K. Bogner, A. Mueller, and P. Salamon. How do I know if my forecasts are better? Using benchmarks in hydrological ensemble prediction. *Journal of Hydrology*, 522:697–713, March 2015.
- [41] R. Msadek, K. W. Dixon, T. L. Delworth, and W. Hurlin. Assessing the predictability of the Atlantic meridional overturning circulation and associated fingerprints: ASSESSING THE PREDICTABILITY OF THE AMOC. *Geophysical Research Letters*, 37(19):n/a–n/a, October 2010.
- [42] Bente Tiedje, Armin Köhl, and Johanna Baehr. Potential predictability of the north atlantic heat transport based on an oceanic state estimate. *Journal of Climate*, 25(24):8475–8486, December 2012.
- [43] Thomas L. Frölicher, Luca Ramseyer, Christoph C. Raible, Keith B. Rodgers, and John Dunne. Potential predictability of marine ecosystem drivers. *Biogeosciences*, 17(7):2061–2083, April 2020.
- [44] Benjamin Buchovecky, Graeme A. MacGilchrist, Mitchell Bushuk, F. Alexander Haumann, Thomas L. Frölicher, Natacha Le Grix, and John Dunne. Potential predictability of the spring bloom in the southern ocean sea ice zone. *Geophysical Research Letters*, 50(20):e2023GL105139, October 2023.
- [45] Roland Séférian, Sarah Berthet, and Matthieu Chevallier. Assessing the decadal predictability of land and ocean carbon uptake. *Geophysical Research Letters*, 45(5):2455–2466, March 2018.
- [46] Aaron Spring and Tatiana Ilyina. Predictability horizons in the global carbon cycle inferred from a perfect-model framework. *Geophysical Research Letters*, 47(9), May 2020.
- [47] Souhail Boussetta, Gianpaolo Balsamo, Gabriele Arduini, Emanuel Dutra, Joe McNorton, Margarita Choulga, Anna Agustí-Panareda, Anton Beljaars, Nils Wedi, Joaquín Muñoz-Sabater, Patricia De Rosnay, Irina Sandu, Ioan Hadade, Glenn Carver, Cinzia Mazzetti, Christel Prudhomme, Dai Yamazaki, and Ervin Zsoter. ECLand: the ECMWF land surface modelling system. *Atmosphere*, 12(6):723, June 2021.
- [48] Michael C. Dietze. Prediction in ecology: a first-principles framework. *Ecological Applications*, 27(7):2048–2060, October 2017.
- [49] James O. Berger and Leonard A. Smith. On the statistical formalism of uncertainty quantification. *Annual Review of Statistics and Its Application*, 6(1):433–460, March 2019.
- [50] Timothy DelSole and Michael K. Tippett. Predictability in a changing climate. *Climate Dynamics*, 51(1-2):531–545, July 2018.
- [51] Kevin Judd, Carolyn A. Reynolds, Thomas E. Rosmond, and Leonard A. Smith. The geometry of model error. *Journal of the Atmospheric Sciences*, 65(6):1749–1772, June 2008.
- [52] Zhichang Guo, Paul A. Dirmeyer, Timothy DelSole, and Randal D. Koster. Rebound in atmospheric predictability and the role of the land surface. *Journal of Climate*, 25(13):4744–4749, July 2012.
- [53] Tilmann Gneiting and Adrian E Raftery. Strictly proper scoring rules, prediction, and estimation. *Journal of the American Statistical Association*, 102(477):359–378, March 2007.
- [54] E. N. Lorenz. Atmospheric predictability experiments with a large numerical model. *Tellus A: Dynamic Meteorology and Oceanography*, 34(6):505, January 1982.
- [55] Y. Qiang Sun and Fuqing Zhang. Intrinsic versus practical limits of atmospheric predictability and the significance of the butterfly effect. *Journal of the Atmospheric Sciences*, 73(3):1419–1438, March 2016.
- [56] I. T. Jolliffe and David B. Stephenson, editors. *Forecast verification: a practitioner's guide in atmospheric science*. J. Wiley, Chichester, West Sussex, England ; Hoboken, NJ, 2003.

- [57] T. M. Hopson. Assessing the ensemble spread–error relationship. *Monthly Weather Review*, 142(3):1125–1142, March 2014.
- [58] Ian T. Jolliffe, editor. *Forecast verification: a practitioner's guide in atmospheric science*. Wiley-Blackwell, Oxford, 2. ed edition, 2012.
- [59] Robert M. May. Simple mathematical models with very complicated dynamics. *Nature*, 261(5560):459–467, June 1976.
- [60] Sam Subbey, Jennifer A. Devine, Ute Schaarschmidt, and Richard D.M. Nash. Modelling and forecasting stock–recruitment: current and future perspectives. *ICES Journal of Marine Science*, 71(8):2307–2322, October 2014.
- [61] Tanya Rogers, Bethany Johnson, and Stephan Munch. Chaos is not rare in natural ecosystems. preprint, In Review, September 2021.
- [62] Werner Rammer, Dominik Thom, Martin Baumann, Kristin Braziunas, Christina Dollinger, Jonas Kerber, Johannes Mohr, and Rupert Seidl. The individual-based forest landscape and disturbance model iLand: Overview, progress, and outlook. *Ecological Modelling*, 495:110785, September 2024.
- [63] Hans Hersbach, Bill Bell, Paul Berrisford, Shoji Hirahara, András Horányi, Joaquín Muñoz-Sabater, Julien Nicolas, Carole Peubey, Raluca Radu, Dinand Schepers, Adrian Simmons, Cornel Soci, Saleh Abdalla, Xavier Abellan, Gianpaolo Balsamo, Peter Bechtold, Gionata Biavati, Jean Bidlot, Massimo Bonavita, Giovanna De Chiara, Per Dahlgren, Dick Dee, Michail Diamantakis, Rossana Dragani, Johannes Flemming, Richard Forbes, Manuel Fuentes, Alan Geer, Leo Haimberger, Sean Healy, Robin J. Hogan, Elías Hólm, Marta Janisková, Sarah Keeley, Patrick Laloyaux, Philippe Lopez, Cristina Lupu, Gabor Radnoti, Patricia De Rosnay, Iryna Rozum, Freja Vamborg, Sebastien Villaume, and Jean-Noël Thépaut. The ERA5 global reanalysis. *Quarterly Journal of the Royal Meteorological Society*, 146(730):1999–2049, July 2020.
- [64] Wouter Dorigo, Irene Himmelbauer, Daniel Aberer, Lukas Schremmer, Ivana Petrakovic, Luca Zappa, Wolfgang Preimesberger, Angelika Xaver, Frank Annor, Jonas Ardö, Dennis Baldocchi, Marco Bitelli, Günter Blöschl, Heye Bogena, Luca Brocca, Jean-Christophe Calvet, J. Julio Camarero, Giorgio Capello, Minha Choi, Michael C. Cosh, Nick Van De Giesen, Istvan Hajdu, Jaakko Ikonen, Karsten H. Jensen, Kasturi Devi Kanniah, Ileen De Kat, Gottfried Kirchengast, Pankaj Kumar Rai, Jenni Kyrouac, Kristine Larson, Suxia Liu, Alexander Loew, Mahta Moghaddam, José Martínez Fernández, Cristian Mattar Bader, Renato Morbidelli, Jan P. Musial, Elise Osenga, Michael A. Palecki, Thierry Pellarin, George P. Petropoulos, Isabella Pfeil, Jarrett Powers, Alan Robock, Christoph Rüdiger, Udo Rummel, Michael Strobel, Zhongbo Su, Ryan Sullivan, Torbern Tagesson, Andrej Varlagin, Mariette Vreugdenhil, Jeffrey Walker, Jun Wen, Fred Wenger, Jean Pierre Wigneron, Mel Woods, Kun Yang, Yijian Zeng, Xiang Zhang, Marek Zreda, Stephan Dietrich, Alexander Gruber, Peter Van Oevelen, Wolfgang Wagner, Klaus Scipal, Matthias Drusch, and Roberto Sabia. The International Soil Moisture Network: serving Earth system science for over a decade. *Hydrology and Earth System Sciences*, 25(11):5749–5804, November 2021.
- [65] Gian Marco Palamara, Francesco Carrara, Matthew J. Smith, and Owen L. Petchey. The effects of demographic stochasticity and parameter uncertainty on predicting the establishment of introduced species. *Ecology and Evolution*, 6(23):8440–8451, December 2016.
- [66] I.M Sobol. Global sensitivity indices for nonlinear mathematical models and their Monte Carlo estimates. *Mathematics and Computers in Simulation*, 55(1-3):271–280, February 2001.
- [67] Jon Herman and Will Usher. SALib: An open-source python library for sensitivity analysis. *The Journal of Open Source Software*, 2(9):97, January 2017.
- [68] Edward N. Lorenz. Predictability - A problem partly solved. 1996.
- [69] Marten Scheffer, Steve Carpenter, Jonathan A. Foley, Carl Folke, and Brian Walker. Catastrophic shifts in ecosystems. *Nature*, 413(6856):591–596, October 2001.
- [70] Sven Erik Jørgensen, editor. *Ecosystem ecology*. Elsevier, Amsterdam, Netherlands ; Boston [Mass.], 1st ed edition, 2009. OCLC: ocn426812909.
- [71] Fuqing Zhang, Y. Qiang Sun, Linus Magnusson, Roberto Buizza, Shian-Jiann Lin, Jan-Huey Chen, and Kerry Emanuel. What is the predictability limit of midlatitude weather? *Journal of the Atmospheric Sciences*, 76(4):1077–1091, April 2019.
- [72] Konrad Bogner, Annie Y.-Y. Chang, Luzi Bernhard, Massimiliano Zappa, Samuel Monhart, and Christoph Spirig. Tercile forecasts for extending the horizon of skillful hydrological predictions. *Journal of Hydrometeorology*, 23(4):521–539, April 2022.

- [73] Francisco J. Doblas-Reyes, Javier García-Serrano, Fabian Lienert, Aida Pintó Biescas, and Luis R. L. Rodrigues. Seasonal climate predictability and forecasting: status and prospects. *WIREs Climate Change*, 4(4):245–268, July 2013.
- [74] Ann Raiho, Michael Dietze, Andria Dawson, Christine R. Rollinson, John Tipton, and Jason McLachlan. Towards understanding predictability in ecology: A forest gap model case study. preprint, *Ecology*, May 2020.
- [75] Peter Bauer, Alan Thorpe, and Gilbert Brunet. The quiet revolution of numerical weather prediction. *Nature*, 525(7567):47–55, September 2015.
- [76] Frank Pennekamp, Matthew W. Adamson, Owen L. Petchey, Jean-Christophe Poggiale, Maíra Aguiar, Bob W. Kooi, Daniel B. Botkin, and Donald L. DeAngelis. The practice of prediction: What can ecologists learn from applied, ecology-related fields? *Ecological Complexity*, 32:156–167, December 2017.
- [77] Bo-Wen Shen, Roger A. Pielke, Xubin Zeng, and Xiping Zeng. Lorenz’s view on the predictability limit of the atmosphere. *Encyclopedia*, 3(3):887–899, July 2023.
- [78] Erica Thompson. *Escape from model land: how mathematical models can lead us astray and what we can do about it*. Basic Books, London, 2022.
- [79] Elisa Benincà, Klaus D. Jöhnk, Reinhard Heerkloss, and Jef Huisman. Coupled predator–prey oscillations in a chaotic food web. *Ecology Letters*, 12(12):1367–1378, December 2009.
- [80] Matthew R. Evans, Mike Bithell, Stephen J. Cornell, Sasha R. X. Dall, Sandra Díaz, Stephen Emmott, Bruno Ernande, Volker Grimm, David J. Hodgson, Simon L. Lewis, Georgina M. Mace, Michael Morecroft, Aristides Moustakas, Eugene Murphy, Tim Newbold, K. J. Norris, Owen Petchey, Matthew Smith, Justin M. J. Travis, and Tim G. Benton. Predictive systems ecology. *Proceedings of the Royal Society B: Biological Sciences*, 280(1771):20131452, November 2013.

THE ECOLOGICAL FORECAST HORIZON REVISITED: POTENTIAL, ACTUAL AND RELATIVE SYSTEM PREDICTABILITY. SUPPLEMENTARY MATERIAL.

Marieke Wesselkamp ¹Jakob Albrecht ²Ewan Pinnington ³William J. Castillo ¹Florian Pappenberger ³Carsten F. Dormann ¹

December 3, 2024

1 Case studies 0 and 1: Stochastic and Coupled Ricker model

1.1 Model description

Ricker equations are used in theoretical ecology to describe functional responses of density-dependent population growth in community structures [?, ?]. In a coupled version they constitute the simplest description of an ecosystem, containing at least one term of interaction with other units, i.e. populations, of the system [?]. Under certain parameter settings, the Ricker equation becomes unstable, resulting in chaotic system behaviour [?]. It's a time-discrete function and for one system component iteratively defined as

$$y_t = y_{t-1} e^{\alpha(1-\beta y_{t-1})} \quad (1)$$

where α is the density independent growth rate and $\beta \cdot y_{t-1}$ the density dependent term. The state variable at any time $t = 1, \dots, \tau$ is the population size y_t which we define relatively to the systems carrying capacity, i.e. standardises it to 1.

Stochastic Ricker model An ensemble of 500 trajectories was simulated by sampling the parameters of the Ricker equation at each time step from uni-variate normal distributions with a variance of $\epsilon = 10\%$ of the parameter size. The β in equation 1 can also be written as $\frac{1}{k}$ where k is the carrying capacity. While we set $k = 1$ for the coupled Ricker model (see below), here we simulated the carrying capacity also stochastically.

$$y_0 = 1 + \sigma_{y_0} \quad (2)$$

$$r \sim \mathcal{N}(0.1, 0.1\epsilon) \quad (3)$$

$$k \sim \mathcal{N}(2, 2\epsilon) \quad (4)$$

$$\sigma_{y_0} \sim \mathcal{N}(0.01, 0.01\epsilon) \quad (5)$$

$$(6)$$

Extended Coupled Ricker model For proof of concept, we use the simplest version of a coupled Ricker model with two interacting populations. We get this model by including a interaction term ν with a dependency on another species

¹Department of Biometry, University of Freiburg, Germany

²Department of Forestry Economics and Forest Planning, University of Freiburg, Germany

³European Center for Medium-Range Weather Forecasts, United Kingdom

Table 1: Parameter meaning and values for the chaotic coupled Ricker model.

Parameter	Meaning	Value
$y_{1,0}$	initial size	1.1
$y_{2,0}$	initial size	1.1
α_1	growth rate	1.29
α_2	growth rate	1.15
β_1	density dependency	1
β_2	density dependency	1
ν_1	interaction	-0.12
ν_2	interaction	-0.13
a_1	-	0.41
a_2	-	0.32
b_1	-	0.31
b_2	-	0.42
σ	population process error	0
σ_x	forcing process error	0.0
l	temporal resolution	200
s	phase shift	0.2

such that one entry of the system of equations Y_t now results in the equation:

$$y_{i,t} = y_{i,t-1} e^{\alpha_i(1 - \beta_i y_{i,t-1} - \nu_i y_{j,t-1})} \quad (7)$$

where i and j indicate row indices of Y_t and Y_t may be simulated with process error as $Y_t = \mathcal{N}(Y_t, \sigma)$. A linear extension that responds to external drivers is considered additively in the exponential part of the model, which allows us to mimic a dependence on seasonality,

$$z_{i,t} = \mathcal{N}(a_i x_t + b_i x_t^2, \sigma_x), \quad (8)$$

where a and b are species-dependent. External drivers x we simulate with a simple cyclic function, i.e. from a sine wave as

$$x = \sin(2\pi \frac{\tau}{l} + \pi s),$$

where l defines the temporal resolution of the temporal cycle, τ the time horizon up to which the forecast is made in resolution of l and s a phase shift on the amplitude of the sine curve.

1.2 Simulation

The model parameters were chosen for demonstration of the potential prognostic predictability on a seasonal case study of the Ricker model with chaotic behaviour (see section 3.1) are listed in table 1.2. These also set the assumptions in the perfect-model framework. A seasonal cycle for simulation of external drivers x consists of 200 time steps. While this is an arbitrary choice that we don't discuss here further, please note that in the unstable parameter regime, the population dynamics are affected by iteration step length. A climatology of ten seasonal cycles was simulated from the model with initial sizes as listed in Table 1.2 and without initial perturbation. The climatological standard deviation σ_c was computed over the full range of the cycle. The PPP evaluates a forecast ensemble based on a perfect-model assumption with only slight perturbation in initial states. As such, the model was initialised 50 times with random draws from a normal distribution $\mathcal{N}(y_0, 0.1)$ for each species, and subsequently the ensemble of models was iterated over one cycle to generate each one member of the seasonal forecast distribution. In a sub-sampling procedure with replacement, the ensemble mean was estimated 50 times on only 40 random draws of the 50 members, estimating the uncertainty around the ensemble mean horizons that are shown in the figure in main manuscript, panel C.

1.3 Lyapunov exponents

Lyapunov exponents were computed based on the Jacobian approach described in the supplementary information to [?].

1.4 Initial time dependence

For creating the plots in the main manuscript, panel C, we ran the analysis from varying initial times over the simulated yearly cycle. A more detailed description of this approach is given in [?].

2 Case study 2: The forest growth model iLand

2.1 Model and variable description

We applied the individual-based forest landscape and disturbance model iLand to demonstrate the actual forecast horizon (see section 3.2) on the example of simulated tree productivity. iLand is a high-resolution, process-based model simulating forest ecosystem processes on multiple scales, from individual trees to landscapes [?]. Here, we only describe model components of particular relevance for simulating tree productivity in managed monospecific stands. Primary production is simulated using a resource-use efficiency model [?] and is driven by daily resolved climate variables (temperature, precipitation, radiation and vapour pressure deficit), atmospheric CO₂ concentration and stable soil conditions (sand, silt and clay fractions, effective soil depth and available nitrogen). Carbohydrate acquisition for each tree is determined by its competitive position for available light. Tree mortality is influenced by the trees age and size as well as its carbon balance (stress-related mortality). Growth, survival, and regeneration in iLand are controlled by 61 species-specific model parameters [?], allowing for the simulation of species' unique responses to environmental changes. iLand was previously parameterized, evaluated and applied for Central European ecosystems [?, ?, ?, ?] and we used the default model parameters from the iLand 1.0 example landscape. Management interventions were implemented using the agent-based forest management model ABE [?], which is fully integrated into the iLand simulation framework. A detailed description of iLand can be found in Seidl et al. (2012a, 2012b) [?, ?] and Rammer et al. (2024) [?]. iLand model code, software and documentation are available online at: <http://ilandmodel.org/>.

2.2 Model initialisation and parameterisation

To initialize and simulate the one-hectare monospecific test stands within the Freiburger Stadtwald information on soils, current vegetation and daily climate was needed (see Table 2.2 for an overview of the variables needed and data sources used). Based on the fine-tuning of a previous study in the Black Forest National Park by Kern et al. (unpublished), the values for plant available nitrogen (nav) and epsilon (ϵ_0), the biome-specific optimum Light Use Efficiency (LUE), were set to 100 kg ha⁻¹ a⁻¹ and 2.1 gC MJ⁻¹, respectively. The carbon cycle was disabled for the simulations.

The climate was represented by observed climate for the period 1951-2020. Historical climate data were extracted from the HYRAS-DE raster dataset [?] and downscaled from 5x5 km to 100x100 m, following Thom et al. (2022) [?]. The method is based on the relationship between climatic variables and elevation. A daily lapse rate for each climate variable is calculated and then used for downscaling each 100x100 m-cell's climate parameters based on the cell's elevation. The CO₂ concentration remained constant over the whole simulation period.

2.3 Simulation

To evaluate tree productivity in managed monospecific stands simulated using iLand, we compared predicted and observed dominant height over a 65-year period. Observations included both point measurements and reconstructions based on yield tables. The dominant height (h100) of a stand is defined as the average height of the 100 largest trees. Initially, stands were identified for which the SI100, the dominant height (h100) at age 100, could be determined. For this purpose, the available inventory plots of the third BWI [?] were used, which are within the Freiburger Stadtwald (only the "Bergwald" inventory plots were available). Each species measured in a plot is assigned with a SI100 using yield tables, which provide a SI100 estimate based on dominant height and age. Based on the SI100 the dominant height growth of each individual tree is reconstructed from yield tables over the whole period. The SI100 derived from the point measurements (observation) defines the yield class of each measured tree. The dominant height growth of the corresponding yield class described in the yield tables is pinned to the point observation to generate a time series. The

Table 2: Overview of variables needed for model initialization.

Variable group	Variables	Data source
Soil	Effective soil depth	[?]
	Soil texture (shares of sand, silt, and clay)	
Climate	Daily temperatures (Min, Max) [°C]	HYRAS-DE v5; HYRAS-DE-RSDS v3 [?]
	Precipitation [mm/day]	
	Solar radiation [MJ/m ² /day]	
	Vapour pressure deficit [kPa]	
Vegetation	Tree count	Yield tables Baden Württemberg FVA-BW (www.fva-bw.de)
	DBH range	
	Height-diameter ratio	
	Age	

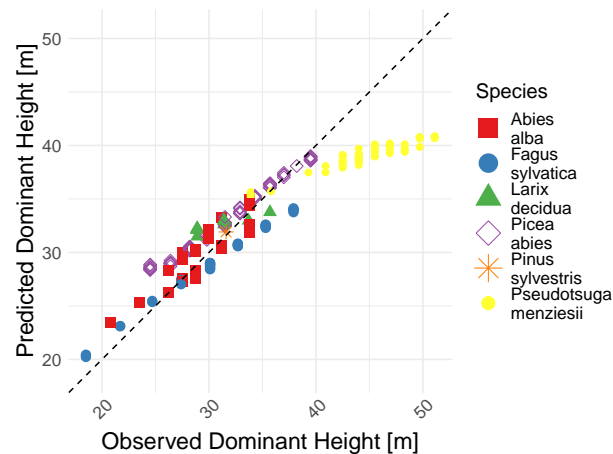


Figure 1: Correlation of observed and simulated dominant heights at age 100.

inventory plots are taken spatially explicit as input stands for iLand, with each plot represented by a 100x100 meter cell, corresponding to a stand for each species at the respective inventory plot. In total 269 (instead of the original 270, we dropped *Pinus Sylvestris* for which only one observation was available) testing stands were modelled, each monospecific and with an observed SH100 as well as reconstructed dominant height growth. The vegetation was initialized at an age of 45 years, based on stand variables (see Table 2.2) derived from the yield tables. The stand development was then simulated with a thinning management applied in five-year intervals, reducing the number of stems per hectare according to the yield tables. For these simulations, the available reference climate data from 1951 to 2016 was used in chronological order.

2.4 Algorithm for determining the forecast horizon

Algorithm 1 Generalized process to receive $\hat{h}(g)$ for all tree species, where g is the observed yield class of a stand.

```

1: for each species in tree species do
2:   Get forecast and observations for species
3:    $\hat{\mathbf{Y}} \leftarrow \text{dominant\_height\_forecast}[\text{species}]$ 
4:    $\mathbf{Y} \leftarrow \text{dominant\_height\_observations}[\text{species}]$ 
5:   for each stand in species_stands do
6:     Select stand
7:      $\hat{y}(g) \leftarrow \hat{\mathbf{Y}}[\text{idx}]$ 
8:      $y(g) \leftarrow \mathbf{Y}[\text{idx}]$ 
9:     Calculate proficiency
10:     $e \leftarrow |y(g) - \hat{y}(g)|$ 
11:     $e_b \leftarrow |y((g \pm \rho_g) - \hat{y}(g))|$ 
12:    Get threshold
13:     $\rho \leftarrow \min_t(e \geq e_b)$ 
14:    Calculate bounded error trajectories  $\mathbf{f}$ 
15:    if  $\rho$  is not infinite then
16:       $\mathbf{f} \leftarrow (\rho - e)$ 
17:    end if
18:  end for
19: end for

```

3 Case study 3: The land surface emulator for ECLand

3.1 Model and variable description

The ECLand emulators that we hereafter refer to as AILand were the testing models, described in [?]. They were parametrised on a European scale with 10-years of (historic) numerical simulations at 6-hourly temporal resolution on a 31 km spatial resolution grid. The details on training and test data and on the parametrisation procedure for the machine learning models, as well as the description of according ECLand simulations that are in this work used as the uninitialised physical model reference can all be found in [?] and its Appendices.

3.2 Evaluation with ISMN observations

AILand was evaluated with in situ soil temperature and soil moisture data that was pre-processed along [?]. These were assembled from ISMN observations of the SMOSMANIA network [?]. As initial time, the 01.02.22, i.e. most recent year was chosen, which required an interval of validation data from the lookback time of the LSTM (23.01.2021) up to the medium-range lead time (14.02.2022). For this time period, 16 of 21 stations had complete time series of soil temperature measurements and 8 stations of soil moisture measurements. For the stations we used, their soil types, see tables 3. For more information, see [?] and [?].

The station data were matched with the according grid cell of the physiographic and climate fields, which were used to force the models during the period. Station data were further resampled to the 6-hourly resolution of the forcing data for evaluation and standardised by z-scoring with the same ECLand prognostic global mean and standard deviation used to train the models in [?].

3.3 Soil moisture experiments

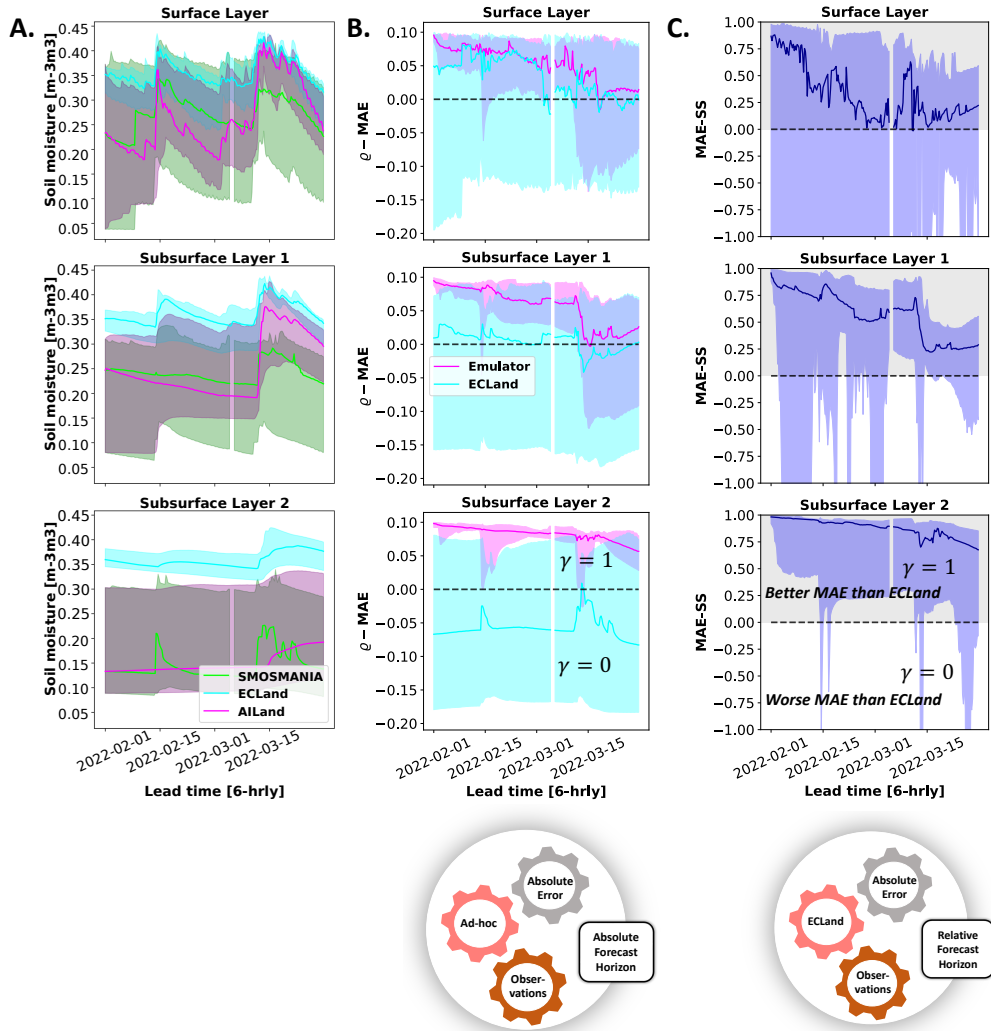


Figure 2: Seasonal-range soil moisture forecasts (A) actual (B) and relative (C) forecast horizons, aggregated over eight of 16 SMOSMANIA stations. 10% of soil water volume was used as error tolerance. Note however, that the actual amount of water percentage strongly varies by soil type and hence requires an individual threshold per station for full interpretability of the actual forecast horizon.

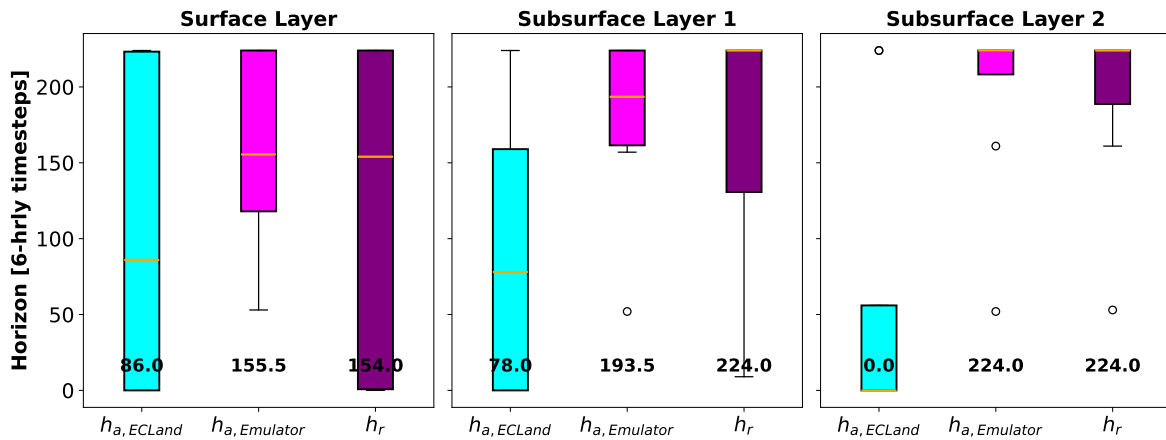


Figure 3: Quantified actual and relative forecast horizons of AILand and ECLand.

Station	Soil Type
Condom	Silty clay
Villevielle	Sandy loam
LaGrandCombe	LaGrandCombe
Narbonne	Clay
Urgons	Silt loam
LezignanCorbieres	Sandy clay loam
CabrieresdAvignon	Sandy clay loam
Savenes	Loam
PeyrusseGrande	Silty clay
Sabres	Sand
Montaut	Montaut
Mazan-Abbaye	Sandy loam
Mouthoumet	Clay loam
Mejannes-le-Clap	Loam
CreondArmagnac	Sand
SaintFelixdeLauragais	Loam

Table 3: SMOSMANIA Stations used for computing soil temperature horizons on three different layers. (<https://doi.org/10.5194/acp-19-5005-2019>)